

# A perfectly matched layer formulation for the nonlinear shallow water equations models: The split equation approach

I.M. Navon

Department of Mathematics and  
Computational Science and Information Technology  
Florida State University  
Tallahassee, FL 32306-4130

B. Neta

Naval Postgraduate School  
Department of Mathematics  
Monterey, CA 93943

M.Y. Hussaini

Computational Science and Information Technology  
Florida State University  
Tallahassee, FL 32306-4120

August 23, 2001

## Abstract

A limited-area model of nonlinear shallow water equations (SWE) with the Coriolis term in a rectangular domain is considered. The rectangular domain is extended to include the so-called perfectly matched layer (PML). Following the proponent of the original method, the PML equations are obtained by splitting the shallow water equations in the coordinate directions and introducing the damping terms. The efficacy of the PML boundary treatment is demonstrated in the case where a Gaussian pulse is initially introduced at the center of the rectangular physical domain. A systematic study is carried out for different mean convection speeds, and various values of the PML width and the damping coefficients. For the purpose of comparison, a reference solution is obtained on a fine grid on the extended domain with the characteristic boundary conditions. The  $L_2$  difference in the height field between the solution with the PML boundary treatment and the reference solution along a line at a downstream position in the interior domain is computed. The PML boundary treatment is found to yield better accuracy compared with both the characteristic boundary conditions and the Engquist-Majda absorbing boundary conditions on an identical grid.

---

<sup>1</sup>Preprint FSU-CSIT-01-41. Submitted to *Monthly Weather Review*.

# 1 Introduction

In a limited-area numerical weather prediction model, the lateral boundaries are not physical boundaries, and they require artificial boundary conditions so that the problem is well-posed and the solution in the limited area remains uncontaminated and consistent with the global solution. As such the treatment of lateral boundaries with the nonreflecting or absorbing boundary conditions has been the subject of continuing interest since the early days of numerical weather prediction.

Several good reviews are available on the topic of both physical and artificial boundary conditions (Givoli and Harari 1998; Turkel 1983 ; Givoli 1991; McDonald 1997; and Tsynkov 1998). Givoli and Harari (1998) have edited a special issue of *Computer Methods in Applied Mechanics and Engineering* on the subject of boundary conditions for exterior wave propagation problems. Turkel (1983) provided an early review on the outflow boundary conditions in the context of computational aerodynamics. Givoli (1991) reviews nonreflecting boundary conditions for the wave problems, discusses local and nonlocal boundary conditions for physical and artificial boundaries in the context of problems from different disciplines. McDonald's (1997) review is confined to lateral boundary conditions for operational regional forecast models. Kalnay (2001) presents the state of art of limited area boundary conditions as used in meteorology. The most comprehensive survey to date of artificial boundary conditions is due to Tsynkov (1998). He provides a comparative assessment of the current methods for constructing the artificial boundary conditions and divides them into two categories – local and global artificial boundary conditions. Local artificial boundary conditions are algorithmically simple but relatively less accurate than the global ones that are highly accurate and robust but computationally expensive if not impractical. His difference potential approach although nonlocal is said to be computationally inexpensive and easy to implement. Any practical algorithm should be a compromise between these two categories. The sponge-layer approach (that includes the PML methodology) may be viewed as a compromise between local and nonlocal approaches. Although it involves no global integral relations along the boundary, a certain amount of nonlocality persists since the computational domain is artificially enlarged to include the sponge layer wherein the model equations are solved using a numerical method close or identical to the one employed in the interior domain.

The approaches of Givoli and Keller (1989) typify the global artificial boundary conditions. They seem to work only in specific geometries and they are obviously not very popular. Typical examples of local approaches to artificial boundary conditions are those of Gustafson and Sundstrom (1978) and Engquist and Majda (1977,1979). These methods can be viewed as a generalization of the Sommerfeld radiation condition and the traditional characteristic boundary conditions. The so-called transparent boundary conditions of McDonald (2001a, 2001b) and of Holstad and Lie (2001) and Lie (2001) applied to the shallow water equations belong to this category.

In the buffer/sponge layer approach, the computational domain is abutted on by the artificial layers in which the waves are either damped or accelerated to supersonic outflow (Perkey and Kreitzberg 1976), Davies (1976), Israeli and Orszag (1981). The boundary relaxation scheme of Davies (1976,1985) is such an approach, and it is most frequently used for limited area forecasting using mesoscale model. Typically the forecast equations at the boundary are modified by the addition of a Newtonian relaxation term that damps the differences between the mesoscale and host model at inflow boundaries while mitigating the effects of overspecification at the outflow boundaries.

The perfectly matched layer (PML) method recently introduced by Berenger (1994) in the context of electromagnetic wave propagation is an improvement on the sponge layer method which has been in vogue in the atmospheric community for almost two decades. The parameters of the PML are chosen such that the wave either never reaches the external boundary, or, even if it reaches the boundary and reflects back, its amplitude is negligibly small by the time it reaches the interface between the sponge layer and interior domain (Clement 1996; Karni 1996; R. Kosloff and D. Kosloff 1986; Hu 1996; Collino 1996; Hayder *et al.* (1999), Hayder and Atkins 1997). The work of Hayder *et al.* (1999) is the first to demonstrate the viability of the PML method in the applications to nonlinear Euler equations. A preliminary work of Darblade *et al.* (1997) implements the PML method to the linearized shallow water equations model in oceanography.

Abarbanel and Gottlieb (1997) provide the general mathematical analysis of the PML method while Abarbanel et al (1999) provide a well posed version of PML for advective acoustics. Abarbanel and Gottlieb (1998) provide the mathematical framework for use of PML in computational acoustics. The well posedness of PML for linearized Euler equation and for the Cauchy problem is discussed in Rahmouni (2000) and Metral and Vacus (1999), respectively. The PML approach has been shown to provide significantly better accuracy than most other artificial boundary conditions in many applications.

The paper is organized as follows. In section 2, we introduce the PML approach to the linearized two-dimensional shallow-water equations for the purpose of analysis. The implications of the split shallow-water model and its weak hyperbolicity are discussed shedding some light on the stability issues of this approach. Reflection and transmission of waves at the interface between two perfectly matched layers is also discussed. Numerical implementation of the PML approach for a limited-area nonlinear shallow water equations model is presented along with the numerical results for the case of a pulse introduced initially at the center of the interior domain. The results are compared with those obtained by employing Engquist-Majda and characteristic boundary conditions. Summary and conclusions are presented in section 3. In the interest of completeness, we provide a brief description of Engquist-Majda approach and the sponge layer approach in the appendix.

## 2 The perfectly matched layer methodology

The perfectly matched layer (PML) technique was first introduced by Berenger (1994) for electromagnetic wave propagation governed by the Maxwell equations. A sponge-layer or medium is introduced in a region adjacent to the artificial boundary of a computational domain.

It is understood that the sponge or buffer-zone solutions themselves need not be physical and they only serve to prevent contamination of the solution in the physical domain by the reflection from the computational boundaries. Usually the absorbing layers are terminated using characteristic boundary conditions. We thus observe a certain analogy between the PML approach and the sponge boundary conditions used previously in meteorology.

In a typical implementation of the PML method, the absorption coefficients in the layer vary spatially in the form:

$$\sigma = \sigma_m \left( \frac{d}{D} \right)^\lambda$$

where  $D$  is the thickness of PML,  $d$  is the distance from the interface with the interior domain and  $\lambda$  is a constant.

In what follows we will develop first the framework of the PML method for the linearized shallow-water (S-W) equations followed by numerical tests on the nonlinear shallow water equations.

### 2.1 Application of the split PML to the linearized S-W equations

The two dimensional linearized S-W equation assumes the form

$$\frac{\partial}{\partial t} u + U \frac{\partial}{\partial x} u + \frac{\partial}{\partial x} \phi = 0 \tag{1}$$

$$\frac{\partial}{\partial t} v + U \frac{\partial}{\partial x} v + \frac{\partial}{\partial y} \phi = 0 \tag{2}$$

$$\frac{\partial}{\partial t} \phi + U \frac{\partial}{\partial x} \phi + c^2 \left( \frac{\partial u}{\partial x} + \frac{\partial v}{\partial y} \right) = 0 \tag{3}$$

where  $u$  and  $v$  are horizontal velocities in the  $x$  and  $y$  directions respectively and  $\phi$  is the geopotential  $\phi = gh$ , where  $H$  is the height of free surface from basic state,  $h$  is a deviation of height from  $H$ , and  $c$  is the phase speed of surface gravity waves, i.e.  $c = \sqrt{gH}$ .

Let us define the following splitting of the fields  $u, v, \phi$  into,  $(u_1, u_2), (v_1, v_2), (\phi_1, \phi_2)$  for the perfectly matched layer:

$$\frac{\partial u_1}{\partial t} + \sigma_x u_1 = -\frac{\partial(\phi_1 + \phi_2)}{\partial x} \quad (4)$$

$$\frac{\partial u_2}{\partial t} + \sigma_x u_2 = -U \frac{\partial(u_1 + u_2)}{\partial x} \quad (5)$$

$$\frac{\partial v_1}{\partial t} + \sigma_y v_1 = -\frac{\partial(\phi_1 + \phi_2)}{\partial y} \quad (6)$$

$$\frac{\partial v_2}{\partial t} + \sigma_x v_2 = -U \frac{\partial(v_1 + v_2)}{\partial x} \quad (7)$$

$$\frac{\partial \phi_1}{\partial t} + \sigma_x \phi_1 = -c^2 \frac{\partial(u_1 + u_2)}{\partial x} - U \frac{\partial(\phi_1 + \phi_2)}{\partial x} \quad (8)$$

$$\frac{\partial \phi_2}{\partial t} + \sigma_y \phi_2 = -c^2 \frac{\partial(v_1 + v_2)}{\partial y} \quad (9)$$

In the above the coefficients  $\sigma_x$  and  $\sigma_y$  have been introduced for the absorption of waves in the PML layer. We will refer to them as absorption coefficients in this work and they will be assumed to be non negative. We notice that when

$$\sigma_x = \sigma_y = 0 \quad (10)$$

we are reduced to the original linearized 2-D shallow-water equations with

$$u = u_1 + u_2 \quad (11)$$

$$v = v_1 + v_2 \quad (12)$$

$$\phi = \phi_1 + \phi_2 \quad (13)$$

The spatial derivatives involve only the total fields of  $u, v$  and  $\phi$  which are assumed to be continuous at the interface between the interior domain and the PML layer.

Two types of interfaces are being created, namely, the interfaces between the interior domain and the PML domain and those between two adjacent PML domains.

We proceed to calculate the wave propagation and absorption properties within a perfectly matched layer followed by the derivation of the reflection and transmission coefficients at the interface between two PML domains for the linearized shallow water equations.

Let a plane wave in the PML domain be expressed as

$$[u_1, u_2, v_1, v_2, \phi_1, \phi_2] = [u_{10}, u_{20}, v_{10}, v_{20}, \phi_{10}, \phi_{20}] e^{i(k_x x + k_y y - \omega t)} \quad (14)$$

the subscripts being used to denote the amplitude of the components. Substituting (14) into (4)-(9) we obtain

$$(\omega + i\sigma_x)u_{10} = k_x(\phi_{10} + \phi_{20}) \quad (15)$$

$$(\omega + i\sigma_x)u_{20} = k_x U(u_{10} + u_{20}) \quad (16)$$

$$(\omega + i\sigma_y)v_{10} = k_y(\phi_{10} + \phi_{20}) \quad (17)$$

$$(\omega + i\sigma_x)v_{20} = k_x U(v_{10} + v_{20}) \quad (18)$$

$$(\omega + i\sigma_x)\phi_{10} = c^2 k_x(u_{10} + u_{20}) + k_x U(\phi_{10} + \phi_{20}) \quad (19)$$

$$(\omega + i\sigma_y)\phi_{20} = c^2 k_y(v_{10} + v_{20}) \quad (20)$$

Let us consider the case when

$$\omega - k_x U + i\sigma_x \neq 0 \quad (21)$$

Then the components in (14) can be expressed as

$$u_{20} = \frac{k_x U}{\omega - k_x U + i\sigma_x} u_{10} \quad (22)$$

$$v_{20} = \frac{k_x U}{\omega - k_x U + i\sigma_x} v_{10} \quad (23)$$

$$\phi_{10} = \frac{c^2 k_x (\omega + i\sigma_x)}{(\omega - k_x U + i\sigma_x)^2} \left( u_{10} + \frac{k_y U}{\omega + i\sigma_y} v_{10} \right) \quad (24)$$

$$\phi_{20} = \frac{c^2 k_y}{\omega - k_x U + i\sigma_x} \frac{\omega + i\sigma_x}{\omega + i\sigma_y} v_{10} \quad (25)$$

We also obtain

$$\left( \frac{\omega + i\sigma_x}{\omega + i\sigma_y} \right) \frac{u_{10}}{v_{10}} = \frac{k_x}{k_y} \quad (26)$$

By substituting expressions for  $\phi_{10}$  and  $\phi_{20}$  into (15) and (17) we obtain

$$u_{10} = \frac{k_x^2 c^2 (\omega + i\sigma_y) u_{10} + c^2 k_x k_y (\omega + i\sigma_x) v_{10}}{(\omega - k_x U + i\sigma_x)^2 (\omega + i\sigma_y)} \quad (27)$$

$$(\omega + i\sigma_y) v_{10} = \frac{c^2 k_x k_y (\omega + i\sigma_y) (\omega + i\sigma_x) u_{10} + c^2 k_y^2 (\omega + i\sigma_x)^2 v_{10}}{(\omega - k_x U + i\sigma_x)^2 (\omega + i\sigma_y)} \quad (28)$$

The 2-D linearized S-W equations dispersion relation (neglecting the Coriolis force) is:

$$(\omega - U k_x)^2 = c^2 (k_x^2 + k_y^2) \quad (29)$$

where an assumption of wave solutions of the form

$$\phi(x, y, t) = \phi_0 e^{i(k_x x + k_y y - \omega t)} \quad (30)$$

is made, i.e.,

$$k_x = \omega \left\{ \frac{U \pm c [1 + (k_y^2 / \omega^2) (U^2 - c^2)]^{1/2}}{U^2 - c^2} \right\} \quad (31)$$

(See Durran *et al.*, 1993). A first-order Taylor expansion of the square root yields:

$$k_x = \frac{\omega}{U \mp c} \pm \frac{c k_y^2}{2\omega} \quad (32)$$

Solving (29) for  $k_y$  yields, after linear approximation of the square root,

$$k_y = \pm \left[ \frac{\omega - U k_x}{c} - \frac{c k_x^2}{2(\omega - U k_x)} \right] \quad (33)$$

For PML we obtain the 2-D shallow-water dispersion relationship in the form:

$$(\omega - k_x U + i\sigma_x)^2 (\omega + i\sigma_y)^2 - k_x^2 c^2 (\omega + i\sigma_y)^2 - k_y^2 c^2 (\omega + i\sigma_x)^2 = 0 \quad (34)$$

This reduces, inside the interior domain where  $\sigma_x = \sigma_y = 0$ , to

$$(\omega - k_x U)^2 \omega^2 = c^2 \omega^2 (k_x^2 + k_y^2) \quad (35)$$

i.e., yielding an identical expression as (29). Collecting  $u_{10}$  terms in (27), dividing by  $\omega + i\sigma_y$  and making use of (26) we get,

$$k_x = \pm(\omega - k_x U + i\sigma_x) \frac{u_{10}}{c\sqrt{u_{10}^2 + v_{10}^2}} \quad (36)$$

Substituting this in (26) we get an expression for  $k_y$  as

$$k_y = \pm(\omega - k_x U + i\sigma_y) \frac{\omega + i\sigma_y}{\omega + i\sigma_x} \frac{v_{10}}{c\sqrt{u_{10}^2 + v_{10}^2}} \quad (37)$$

If  $u_{10}/v_{10}$  is real for solution of the S-W equations then one could express  $u_{10}$  and  $v_{10}$  as

$$u_{10} = A \cos \Phi \quad (38)$$

$$v_{10} = A \sin \Phi \quad (39)$$

where  $A$  is a complex number and  $\Phi$  is a real number. If we substitute (38) and (39) into (36) and (37) and we solve for  $k_x$  and  $k_y$ , we obtain (by taking only the + sign)

$$k_x = \frac{(\omega + i\sigma_x)}{c + U \cos \Phi} \cos \Phi \quad (40)$$

$$k_y = \frac{(\omega + i\sigma_y)}{c + U \cos \Phi} \sin \Phi \quad (41)$$

Using these expressions we can simplify expressions (22)-(25) so as to get the plane wave solutions to (15)-(20) to be expressed as

$$\begin{bmatrix} u_1 \\ u_2 \\ v_1 \\ v_2 \\ \phi_1 \\ \phi_2 \end{bmatrix} = A \begin{bmatrix} \cos \Phi \\ U/c \cos^2 \Phi \\ \sin \Phi \\ U/c \cos \Phi \sin \Phi \\ c \cos^2 \Phi + U \cos \Phi \\ c \sin^2 \Phi \end{bmatrix} e^{i\omega \left( \frac{\cos \Phi}{c + U \cos \Phi} x + \frac{\sin \Phi}{c + U \cos \Phi} y - t \right)} \times \quad (42)$$

$$e^{\left( -\frac{\sigma_x \cos \Phi}{c + U \cos \Phi} x - \frac{\sigma_y \sin \Phi}{c + U \cos \Phi} y \right)}$$

This expression represents a wave propagating with gravity wave speed relative to the mean flow and making an angle  $\Phi$  with the  $x$  axis. When both  $\sigma_x$  and  $\sigma_y \neq 0$ , the magnitude of the wave decreases exponentially as it propagates in either the  $x$  or  $y$  directions, respectively.

## 2.2 Weak hyperbolicity of the split PML

### 2.2.1 Analysis of the linearized S-W equations

The 2-D linearized shallow water model assumes the form

$$\frac{\partial}{\partial t} u + U \frac{\partial}{\partial x} u + \frac{\partial}{\partial x} \phi - f v = 0 \quad (43)$$

$$\frac{\partial}{\partial t} v + U \frac{\partial}{\partial x} v + \frac{\partial}{\partial y} \phi + f u = 0 \quad (44)$$

$$\frac{\partial}{\partial t} \phi + U \frac{\partial}{\partial x} \phi + c^2 \left( \frac{\partial u}{\partial x} + \frac{\partial v}{\partial y} \right) = 0 \quad (45)$$

We can write the system as

$$\frac{\partial W}{\partial t} + A \frac{\partial W}{\partial x} + B \frac{\partial W}{\partial y} + C W = 0$$

where the vector  $W$  is

$$\begin{bmatrix} u \\ v \\ \frac{1}{c}\phi \end{bmatrix}$$

and the matrices  $A, B$  and  $C$  are

$$A = \begin{bmatrix} U & 0 & c \\ 0 & U & 0 \\ c & 0 & U \end{bmatrix}$$

$$B = \begin{bmatrix} 0 & 0 & 0 \\ 0 & 0 & c \\ 0 & c & 0 \end{bmatrix}$$

$$C = \begin{bmatrix} 0 & -f & 0 \\ f & 0 & 0 \\ 0 & 0 & 0 \end{bmatrix}$$

Since  $A$  and  $B$  are symmetric and the equation is hyperbolic, the system is strongly well-posed (Gustafson and Sundstrom, 1978)

### 2.2.2 Analysis of the split-PML linearized shallow water equations including the Coriolis factor

The 2-D linearized shallow water model assumes the form (43)-(45). If we include the absorption coefficients for the PML prior to the splitting we have:

$$\frac{\partial}{\partial t}u + U\frac{\partial}{\partial x}u + \frac{\partial}{\partial x}\phi - fv = -\sigma_u u \quad (46)$$

$$\frac{\partial}{\partial t}v + U\frac{\partial}{\partial x}v + \frac{\partial}{\partial y}\phi + fu = -\sigma_v v \quad (47)$$

$$\frac{\partial}{\partial t}\phi + U\frac{\partial}{\partial x}\phi + c^2\left(\frac{\partial u}{\partial x} + \frac{\partial v}{\partial y}\right) = -\sigma_\phi \phi \quad (48)$$

The inclusion of the Coriolis factor in the nonlinear shallow-water equations requires the following modification of the PML split form:

$$\begin{aligned} \frac{\partial u_1}{\partial t} + \frac{\partial \phi}{\partial x} &= -\sigma_x u_1 \\ \frac{\partial u_2}{\partial t} + U\frac{\partial u}{\partial x} &= -\sigma_x u_2 \\ \frac{\partial u_3}{\partial t} - fv &= 0 \\ \frac{\partial v_1}{\partial t} + \frac{\partial \phi}{\partial y} &= -\sigma_y v_1 \\ \frac{\partial v_2}{\partial t} + U\frac{\partial v}{\partial x} &= -\sigma_x v_2 \end{aligned} \quad (49)$$

with  $\phi = \phi_1 + \phi_2$ ,  $u = u_1 + u_2 + u_3$  and  $v = v_1 + v_2 + v_3$ . A similar approach was used for the linearized shallow-water equations in oceanography by Darblade *et al.* (1997).

These equations can be written as

$$\frac{\partial W^s}{\partial t} + A^s \frac{\partial W^s}{\partial x} + B^s \frac{\partial W^s}{\partial y} + C^s W^s = 0$$

where the vector  $W^s$  is defined as

$$\left[ u_1 \quad u_2 \quad u_3 \quad v_1 \quad v_2 \quad v_3 \quad \frac{1}{c}\phi_1 \quad \frac{1}{c}\phi_2 \right]^T$$

and the matrices  $A^s$ ,  $B^s$  and  $C^s$  are

$$A^s = \begin{bmatrix} 0 & 0 & 0 & 0 & 0 & 0 & c & c \\ U & U & U & 0 & 0 & 0 & 0 & 0 \\ 0 & 0 & 0 & 0 & 0 & 0 & 0 & 0 \\ 0 & 0 & 0 & 0 & 0 & 0 & 0 & 0 \\ 0 & 0 & 0 & U & U & U & 0 & 0 \\ 0 & 0 & 0 & 0 & 0 & 0 & 0 & 0 \\ c & c & c & 0 & 0 & 0 & U & U \\ 0 & 0 & 0 & 0 & 0 & 0 & 0 & 0 \end{bmatrix}$$

$$B^s = \begin{bmatrix} 0 & 0 & 0 & 0 & 0 & 0 & 0 & 0 \\ 0 & 0 & 0 & 0 & 0 & 0 & 0 & 0 \\ 0 & 0 & 0 & 0 & 0 & 0 & 0 & 0 \\ 0 & 0 & 0 & 0 & 0 & 0 & c & c \\ 0 & 0 & 0 & 0 & 0 & 0 & 0 & 0 \\ 0 & 0 & 0 & 0 & 0 & 0 & 0 & 0 \\ 0 & 0 & 0 & 0 & 0 & 0 & 0 & 0 \\ 0 & 0 & 0 & c & c & c & 0 & 0 \end{bmatrix}$$

$$C^s = \begin{bmatrix} \sigma_x & 0 & 0 & 0 & 0 & 0 & 0 & 0 \\ 0 & \sigma_x & 0 & 0 & 0 & 0 & 0 & 0 \\ 0 & 0 & 0 & -f & -f & -f & 0 & 0 \\ 0 & 0 & 0 & \sigma_y & 0 & 0 & c & c \\ 0 & 0 & 0 & 0 & \sigma_x & 0 & 0 & 0 \\ f & f & f & 0 & 0 & 0 & 0 & 0 \\ 0 & 0 & 0 & 0 & 0 & 0 & \sigma_x & 0 \\ 0 & 0 & 0 & 0 & 0 & 0 & 0 & \sigma_y \end{bmatrix}$$

The matrix  $S$  that diagonalizes  $A^s$  is

$$S = \begin{bmatrix} -1 & -1 & 0 & 0 & 0 & 0 & -\frac{c}{U} & 1 \\ 1 & 0 & 0 & 0 & 0 & 0 & 1 & \frac{U}{c} \\ 0 & 1 & 0 & 0 & 0 & 0 & 0 & 0 \\ 0 & 0 & -1 & 0 & -1 & 0 & 0 & 0 \\ 0 & 0 & 1 & 0 & 0 & 1 & 0 & 0 \\ 0 & 0 & 0 & 0 & 1 & 0 & 0 & 0 \\ 0 & 0 & 0 & -1 & 0 & 0 & \frac{c-U}{U} & \frac{c+U}{c} \\ 0 & 0 & 0 & 1 & 0 & 0 & 0 & 0 \end{bmatrix}$$

The inverse is

$$S^{-1} = \begin{bmatrix} \frac{U^2}{c^2 - U^2} & \frac{c^2}{c^2 - U^2} & \frac{U^2}{c^2 - U^2} & 0 & 0 & 0 & -\frac{Uc}{c^2 - U^2} & -\frac{Uc}{c^2 - U^2} \\ 0 & 0 & 1 & 0 & 0 & 0 & 0 & 0 \\ 0 & 0 & 0 & -1 & 0 & -1 & 0 & 0 \\ 0 & 0 & 0 & 0 & 0 & 0 & 0 & 1 \\ 0 & 0 & 0 & 0 & 0 & 1 & 0 & 0 \\ 0 & 0 & 0 & 1 & 1 & 1 & 0 & 0 \\ -\frac{1}{2} \frac{U}{c - U} & -\frac{1}{2} \frac{U}{c - U} & -\frac{1}{2} \frac{U}{c - U} & 0 & 0 & 0 & \frac{1}{2} \frac{U}{c - U} & \frac{1}{2} \frac{U}{c - U} \\ \frac{1}{2} \frac{c}{c + U} & \frac{1}{2} \frac{c}{c + U} & \frac{1}{2} \frac{c}{c + U} & 0 & 0 & 0 & \frac{1}{2} \frac{c}{c + U} & \frac{1}{2} \frac{c}{c + U} \end{bmatrix}$$

It is easy to show that

$$S^{-1}A^sS = \begin{bmatrix} 0 & 0 & 0 & 0 & 0 & 0 & 0 & 0 \\ 0 & 0 & 0 & 0 & 0 & 0 & 0 & 0 \\ 0 & 0 & 0 & 0 & 0 & 0 & 0 & 0 \\ 0 & 0 & 0 & 0 & 0 & 0 & 0 & 0 \\ 0 & 0 & 0 & 0 & 0 & 0 & 0 & 0 \\ 0 & 0 & 0 & 0 & 0 & U & 0 & 0 \\ 0 & 0 & 0 & 0 & 0 & 0 & U - c & 0 \\ 0 & 0 & 0 & 0 & 0 & 0 & 0 & U + c \end{bmatrix}$$

Note that  $S^{-1}A^sS$  is a diagonal matrix with 5 zero eigenvalues being introduced as a result of the splitting. It is straightforward to show that these five additional eigenvalues imply that  $S$  and  $S^{-1}$  cannot transform  $B^s$  into a matrix that can be made symmetric by multiplication with a positive definite diagonal matrix (see Hesthaven 1998). The most general diagonalizer of  $A^s$  is  $S = TR$  (Abarbanel 1999) where the columns of  $T$  are the eigenvectors of  $A^s$  and  $R$  is a matrix such that the columns of  $S$  are the most general representation of the eigenvectors of  $A^s$ .

### 2.3 Reflection and transmission at an interface between two perfectly matched layers

Let us consider the wave reflection and transmission at an interface between two PML domains. This includes the interface between the interior limited area domain and the PML domain. The absorbing coefficients  $\sigma_x$  and  $\sigma_y$  will be chosen such that  $\sigma_y$  is the same across the interface normal to  $y$ .

The linearized S-W equations can be viewed as the split field PML linearized S-W equations with both absorption coefficients being zero across an interface normal to  $x$  and  $y$  between an interior domain and a PML domain. To illustrate this we present in the following diagram the absorption coefficients on a corner of the computational domain.

<i>PML</i>	$(0, \sigma_y)$	$(\sigma_x, \sigma_y)$
	$(0, 0)$	$(\sigma_x, 0)$
	interior	<i>PML</i>

We will show that reflection coefficient at an interface downstream normal to  $x$  is zero for incident gravity waves, a result that carries over for the interfaces. Let the interface be located downstream at  $x = 0$  and let absorption coefficients be denoted by  $\sigma_{x1}$  and  $\sigma_y$  on one side of it and  $\sigma_{x2}$  and  $\sigma_y$  on the other. We consider incident, reflected and transmitted waves.

a. Incident wave

$$\begin{pmatrix} u_1 \\ u_2 \\ v_1 \\ v_2 \\ \phi_1 \\ \phi_2 \end{pmatrix} = A_i \begin{pmatrix} \cos \Phi_i \\ (U/c) \cos \Phi_i \\ \sin \Phi_i \\ (U/c) \cos \Phi_i \sin \Phi_i \\ c \cos^2 \Phi_i + U \cos \Phi_i \\ c \sin^2 \Phi_i \end{pmatrix} e^{i\omega \left( \frac{\cos \Phi_i}{c+U \cos \Phi_i} x + \frac{\sin \Phi_i}{c+U \cos \Phi_i} y - t \right)} \times e^{\left( -\frac{\sigma_{x1} \cos \Phi_i}{c+U \cos \Phi_i} x - \frac{\sigma_y \sin \Phi_i}{c+U \cos \Phi_i} y \right)} \quad (50)$$

b. Reflected wave

$$\begin{pmatrix} u_1 \\ u_2 \\ v_1 \\ v_2 \\ \phi_1 \\ \phi_2 \end{pmatrix} = A_i \begin{pmatrix} -\cos \Phi_r \\ (U/c) \cos \Phi_r \\ \sin \Phi_r \\ -(U/c) \cos \Phi_r \sin \Phi_r \\ c \cos^2 \Phi_r - U \cos \Phi_r \\ c \sin^2 \Phi_r \end{pmatrix} e^{i\omega \left( \frac{-\cos \Phi_r}{c-U \cos \Phi_r} x + \frac{\sin \Phi_r}{c-U \cos \Phi_r} y - t \right)} \times e^{\left( \frac{\sigma_{x1} \cos \Phi_r}{c-U \cos \Phi_r} x - \frac{\sigma_y \sin \Phi_r}{c-U \cos \Phi_r} y \right)} \quad (51)$$

c. Transmitted wave

$$\begin{pmatrix} u_1 \\ u_2 \\ v_1 \\ v_2 \\ \phi_1 \\ \phi_2 \end{pmatrix} = A_i \begin{pmatrix} \cos \Phi_t \\ (U/c) \cos \Phi_t \\ \sin \Phi_t \\ (U/c) \cos \Phi_t \sin \Phi_t \\ c \cos^2 \Phi_t + U \cos \Phi_t \\ c \sin^2 \Phi_t \end{pmatrix} e^{i\omega \left( \frac{\cos \Phi_t}{c+U \cos \Phi_t} x + \frac{\sin \Phi_t}{c+U \cos \Phi_t} y - t \right)} \times e^{\left( -\frac{\sigma_{x2} \cos \Phi_t}{c+U \cos \Phi_t} x - \frac{\sigma_y \sin \Phi_t}{c+U \cos \Phi_t} y \right)} \quad (52)$$

The transmitted wave can have another component of

$$\omega - k_x U + i\sigma_x = 0 \quad (53)$$

in which case

$$k_x = \frac{\omega + i\sigma_x}{U} \quad (54)$$

It also follows  $u_{10} = v_{10} = 0$  and from (15), (17)

$$\phi_{10} + \phi_{20} = 0 \quad (55)$$

One can express  $u_{20}$  and  $v_{20}$  as

$$u_{20} = -B \sin \psi \quad (56)$$

$$v_{20} = B \cos \psi \quad (57)$$

For  $k_y$  one obtains upon dividing (19) by (20) and using (54)-(57)

$$k_y = \frac{\omega + i\sigma_y}{U} \tan \psi \quad (58)$$

So in this case the plane wave solutions will take form

$$\begin{pmatrix} u_1 \\ u_2 \\ v_1 \\ v_2 \\ \phi_1 \\ \phi_2 \end{pmatrix} = \begin{pmatrix} 0 \\ -B \sin \psi \\ 0 \\ B \cos \psi \\ -Bc^2 \sin \psi / U \\ Bc^2 \sin \psi / U \end{pmatrix} e^{i\omega \left( \frac{1}{U}x + \frac{\tan \psi}{U}y - t \right)} e^{(-\frac{\sigma_x}{U}x - \frac{\sigma_y \tan \psi}{U}y)} \quad (59)$$

Thus the transmitted wave may have a component

$$\begin{pmatrix} 0 \\ -B_t \sin \psi_t \\ 0 \\ B_t \cos \psi_t \\ -B_t c^2 \sin \psi_t / U \\ B_t c^2 \sin \psi_t / c \end{pmatrix} e^{i\omega \left( \frac{1}{U}x + \frac{\tan \psi_t}{U}y - t \right)} e^{(-\frac{\sigma_x}{U}x - \frac{\sigma_y \tan \psi_t}{U}y)} \quad (60)$$

At the interface we impose continuity conditions, i.e. that  $u_1 + u_2$ ,  $v_1 + v_2$ , and  $\phi_1 + \phi_2$  be continuous.

Since continuity is valid for all values of  $y$  at the interface it follows that the coefficients of  $y$  in the exponents of (a), (b), (c) (incident, reflected and transmitted values), must be the same.

This yields

$$\frac{\sin \Phi_r}{c - U \cos \Phi_r} = \frac{\sin \Phi_i}{c + U \cos \Phi_i} \quad (61)$$

$$\frac{\sin \Phi_t}{c + U \cos \Phi_t} = \frac{\sin \phi_i}{c + U \cos \Phi_i} \quad (62)$$

$$\tan \psi_t = \tan \psi_i \quad (63)$$

We assume

$$\frac{\tan \psi_i}{U} = \frac{\sin \Phi_i}{c + U \cos \psi_i}. \quad (64)$$

We then find from the above that

$$\Phi_r = 2 \tan^{-1} \left( \frac{1 - U}{1 + U} \tan \frac{\Phi_i}{2} \right) \quad (65)$$

$$\Phi_t = \Phi_i \quad (66)$$

$$\psi_t = \psi_i \quad (67)$$

Using the continuity of  $u_1 + u_2$ ,  $v_1 + v_2$  and  $\phi_1 + \phi_2$  we have,

$$\begin{aligned} A_i(c + U \cos \Phi_i) \cos \Phi_i &- A_r(c - U \cos \Phi_r) \cos \Phi_r - B_i \sin \psi_i \\ &= A_t(c + U \cos \Phi_t) \cos \Phi_t - B_t \sin \psi_t \end{aligned} \quad (68)$$

$$\begin{aligned} A_i(c + U \cos \Phi_i) \sin \Phi_i &+ A_r(c - U \cos \Phi_r) \sin \Phi_r + B_i \cos \psi_i \\ &= A_t(c + U \cos \Phi_t) \sin \Phi_t + B_t \cos \psi_t \end{aligned} \quad (69)$$

$$A_i(c + U \cos \Phi_i) + A_r(c - U \cos \Phi_r) = A_t(c + U \cos \Phi_t) \quad (70)$$

Using (65)-(67), the above 3 equations may be rewritten as a linear system of 3 homogeneous equations for  $A_i - A_t$ ,  $A_r$ , and  $B_i - B_t$ , provided the coefficient determinant is different from zero. A straightforward but lengthy calculation shows that the coefficient determinant is not zero for any angle of incidence. Thus the only solution is the trivial one, i.e.  $A_r = 0$ ,  $A_t = A_i$ , and  $B_t = B_i$ . Thus for the linearized S-W equations at

the interface between two PML domains downstream normal to the  $x$ -axis with PML absorption coefficients  $(\sigma_{x1}, \sigma_y)$ ,  $(\sigma_{x2}, \sigma_y)$  we get null reflection while transmitted waves will maintain same direction and amplitude as the incident waves. This result is subject to the restrictions imposed by assumptions of linearity. Since it has been shown by Hu (1996), Tam *et al.* (1998), and Abarbanel *et al.* (1999) that the PML approach is only weakly stable, a low pass filter of the form

$$1 - \sin^{10} \left( \frac{k\Delta x}{2} \right) \quad (71)$$

where  $k$  is the wave number and  $\Delta x$  the grid spacing has been used in the aforementioned references.

In practical applications of the PML method a gradually varying absorption coefficient of the form

$$\sigma = \sigma_m \left( \frac{d}{D} \right)^\beta \quad (72)$$

is used where  $D$  is the thickness of the PML domain and  $d$  is the distance from interface with interior domain. If we apply at the end of the PML domain a radiation boundary condition, then the wave is reflected and upon reflection in the domain its total reflection factor is expressed as

$$e^{-\frac{2\sigma_m D}{\beta+1} \frac{\cos \Phi}{c^2 - U^2 \cos^2 \Phi}} \quad (73)$$

for gravity waves and for Rossby waves it can be estimated as

$$e^{-\frac{\sigma_m D}{U(\beta+1)}} \quad (74)$$

In experiments with linearized Euler equations a gradual  $\sigma$  variation was used with a value of

$$\frac{\sigma_m D}{\beta+1} \approx 8 \quad (75)$$

Usually a value of  $\beta \approx 3$  is taken, i.e.  $\sigma_m D = 32$ . We will use these values as guidelines for our numerical experiments.

## 2.4 Numerical implementation considerations

A 2-D nonlinear shallow-water equations solver based on the explicit Miller-Pearce finite difference scheme is used (Miller and Pearce 1974). The scheme has a CFL stability condition

$$\Delta t \leq \frac{\Delta x}{c}$$

where  $c$  is the speed of external gravity waves. Spatial differencing of the nonlinear shallow water equations was carried out on a rectangular domain of  $61 \times 61$  grid points, with a spatial horizontal grid length of  $\Delta x = \Delta y = 20km$ .

To demonstrate the implementation of the PML equations we used a number of variable thickness stencils of the PML region - thus allowing a gradual variation in the PML domain.

At the outer boundary of the PML domain we apply characteristic boundary conditions.

We compared the results with a control simulation computed on a much larger domain i.e. a domain of  $[-240, 240] \times [-240, 240]$  which is not affected by the boundary conditions for the integration time span. The interior domain where the unaltered nonlinear shallow-water equations are applied is  $[-20, 20] \times [-20, 20]$ .

To assess the accuracy of the proposed scheme, we have computed either the maximum error in the height field along the line  $x = 18$  inside the inner domain as a function of time. This is done both in the infinity

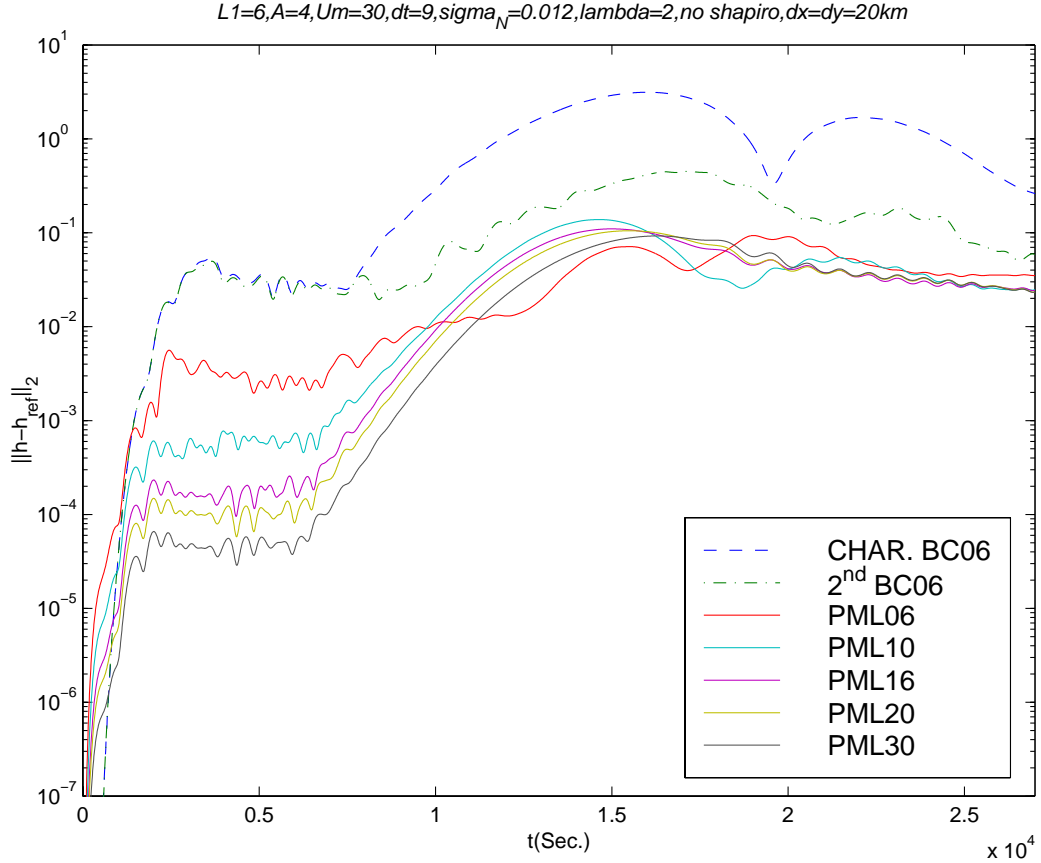


Figure 1: The evolution of the  $L_2$  height error along the line  $x = 18$  for various PML layer thicknesses for  $U_m = 30m/sec$ . The error computing only characteristic or second order Engquist-Majda boundary conditions is given for comparison.

norm as well as in the  $L_2$  norm. This allows us to verify the efficiency of the PML absorbing layer as a function of the width of the layer. Characteristic shallow water boundary conditions are used to terminate the PML layer domain.

We observe that even for a PML layer of thickness of only  $6\Delta x$ , the PML scheme outlined above outperforms the characteristic boundary conditions, while increasing the width of the PML layer leads to a significant increase in accuracy.

The present results are without the use of filtering, despite the fact that linear analysis of the scheme points to weak well-posedness (Hesthaven 1998). As expected the height field wave propagates undisturbed from the computational domain with no visible reflections. The main result obtained is that we solve the PML split version for the nonlinear shallow water equations and the results show that the split scheme including the Coriolis factor is stable thus confirming the decaying properties of fields inside the PML layer.

The  $L_2$  norm difference between the computed and reference solutions along a line inside the inner domain two grid points away from the PML boundary namely at  $x = 18$  (in absolute distance) is presented in Figure 1 as a function of time. This measures the magnitude of the reflected wave at the outflow boundary. PML domains whose thickness are 6, 10, 12, 14, 16, 20 and 30 grid points have been used in the numerical experiments described below.

The initial conditions are :

$$h = h_{av} + Ae^{-\frac{(x-x_0)^2 + (y-y_0)^2}{L^2}}, \quad (76)$$

$$u = 2\frac{g}{f_0}A\frac{y-y_0}{L^2}e^{-\frac{(x-x_0)^2 + (y-y_0)^2}{L^2}}, \quad (77)$$

$$v = -2\frac{g}{f_0}A\frac{x-x_0}{L^2}e^{-\frac{(x-x_0)^2 + (y-y_0)^2}{L^2}}, \quad (78)$$

where  $A$  is the amplitude,  $(x_0, y_0)$  is the initial center of Gaussian vortex,  $h_{av}$  is a reference height,  $f_0$  being the Coriolis parameter at a reference latitude.

## 2.5 Results

Here we report on the results of our numerical experiments with various values of mean flow speeds and absorption coefficients for the PML layer. In all experiments we let the center of the Gaussian be at the origin, i.e.  $(x_0, y_0) = (0, 0)$ , the Gaussian amplitude is  $A = 6$  and  $L = 4$ . In the first experiment the PML parameters are  $\beta = 2$  and  $\sigma_m = 0.0012$ . The mean flow speed varied from  $U_m = 0m/sec$  to  $U_m = 100m/sec$ .

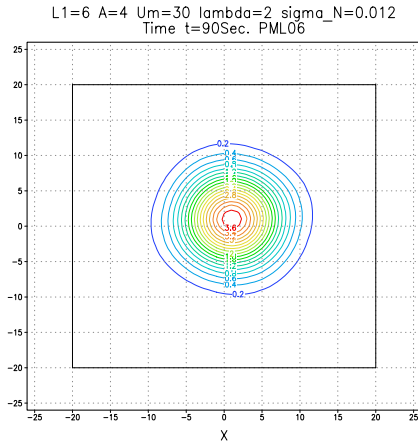
In figures 1-2(c) we take  $U_m = 30m/sec$ . Figure 1 shows the  $L_2$  error in the height field between the PML layer domain and the reference solution along a line located inside the interior domain, two grid points away from the PML layer boundary. For comparison we present the results obtained with models having different values of the thickness of the PML layer ( $6\Delta x$ - $30\Delta x$ ) as well as results arrived at using only characteristic variables or results obtained using the second order Engquist boundary conditions.

From Figure 1 we note that, during a first stage, the  $L_2$  error differences for all the various layer thicknesses start by growing up quickly, while at the second stage, they display a tendency to flatten out, after about 7000 seconds, while at the third stage, they grow up again attaining a size of the order of  $10^{-2}$ , and become constant thereafter (this is related to the exit of the Gaussian vortex from the model domain). The errors computed using only the characteristic boundary conditions and the second order Engquist boundary conditions are given for comparison. The depth of PML layer obviously impacts on the results, namely the thicker the PML layer is, the better are the results achieved. In the same figure, it can also be seen that all the results for the PML layers of various thicknesses are better than those obtained by either the characteristic boundary condition (highest dashed line) or second order Engquist boundary conditions (second highest line).

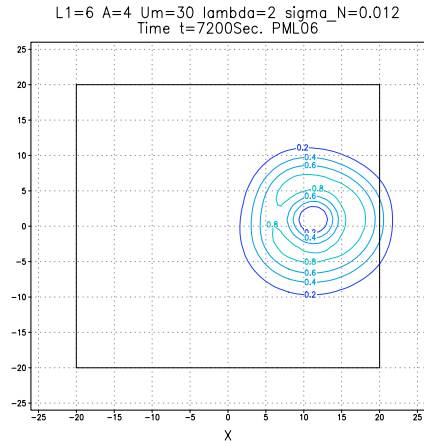
The time history of the Gaussian pulse transported by the mean flow and propagating towards the right boundary is presented in Figures 2(a) - 2(c) in terms of height contours. Figure 2(a) shows the contour lines initially, while Figure 2(b) shows the contours when the outer edge of the Gaussian reaches the PML boundary. Figure 2(c) shows the vortex passing through the PML layer. One notes that the Gaussian vortex passes without reflection through the PML boundary. In the PML region, the contours are deformed, since their amplitudes are reduced towards the outer boundary.

In the next experiment we have increased the mean flow speed to  $U_m = 40m/sec$ . Figure 3 shows the evolution of the  $L_2$  error along the same vertical line inside the interior domain, two grid points away from the PML layer boundary. The results are similar to those obtained with  $U_m = 30m/sec$ , however the times at which the different stages are attained differ, due to faster movement of the Gaussian vortex towards the right boundary. Again when using the characteristic boundary conditions or the second order Engquist boundary conditions we get larger  $L_2$  errors.

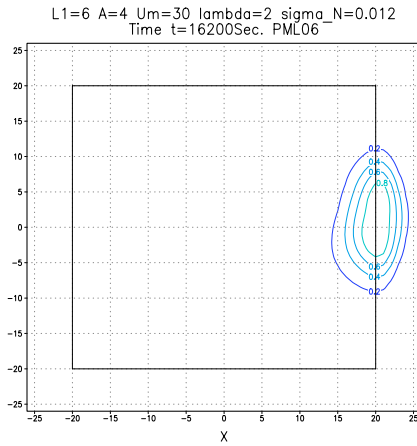
The time history of the Gaussian pulse transported by the mean flow and propagating towards the right boundary is presented in Figures 4(a) - 4(c) in terms of height contours. Figure 4(a) shows the contour lines at the initial time, while Figure 4(b) shows the contours when the outer edge of the Gaussian reaches the PML boundary. Figure 4(c) shows the vortex passing through the PML layer. Again one notes that the Gaussian vortex passes without reflection through the PML boundary. In the PML region, the contours are deformed, since their amplitudes are reduced towards the outer boundary.



(a) Height contours for the Gaussian profile propagating with convective mean velocity of  $U_m = 30m/sec$ . The computed result is given at  $t = 90sec$ . for a PML layer thickness of 6 grid points.



(b) Same as Fig. 2(a) but the computed result is at  $t = 720sec$ .



(c) Same as Fig. 2(a) but the computed result is at  $t = 16200sec$ .

Figure 2:

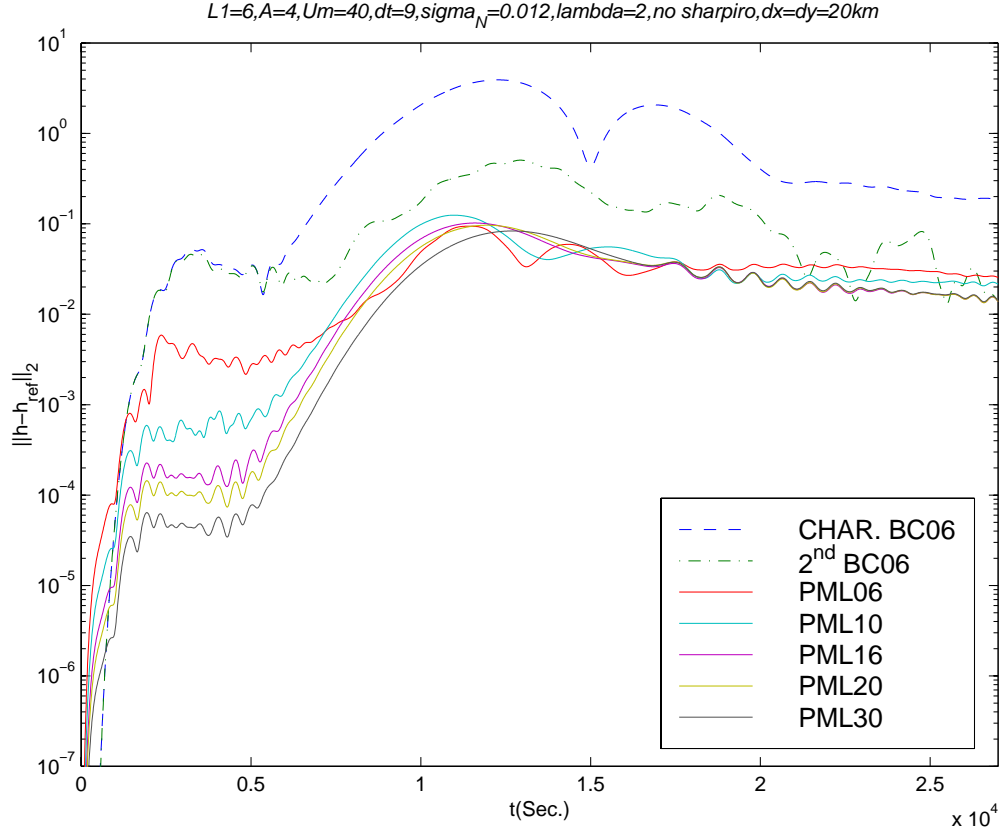


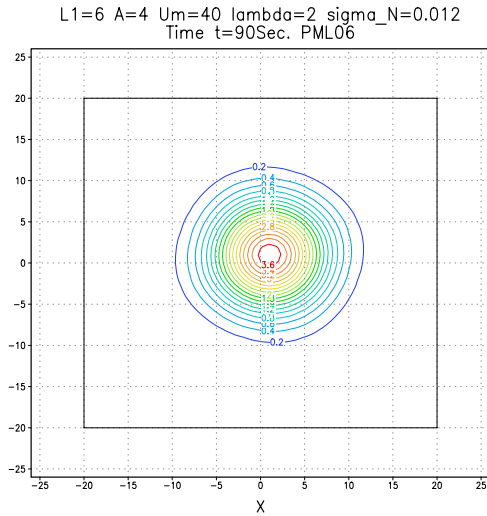
Figure 3: The evolution of the  $L_2$  height error along the line  $x = 18$  for various PML layer thicknesses for  $U_m = 40\text{m}/\text{sec}$ . The error computing only characteristic or second order E-M boundary conditions is given for comparison.

The next experiment takes a high mean flow speed of  $U_m = 100\text{m}/\text{sec}$ . Figure 5 show a comparative  $L_2$  error norm in the height field. For this high mean flow speed strong oscillations are noticed for the PML layer model after 15000 seconds, when the vortex has moved out of PML region. Again the errors are largest when using either the characteristic boundary conditions or the Engquist boundary conditions.

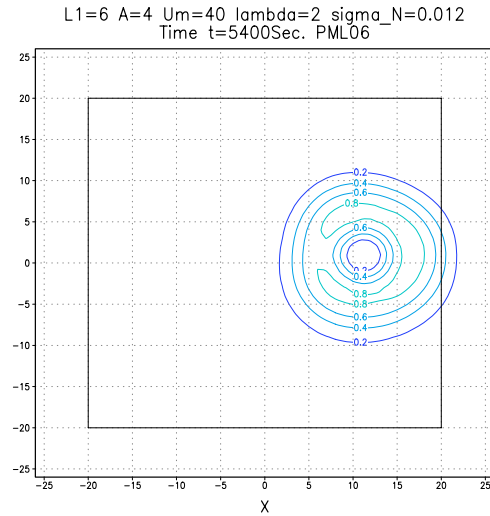
The time history of the Gaussian pulse transported by the high mean flow speed of  $U_m = 100\text{m}/\text{sec}$  and propagating towards the right boundary is presented in Figures 6(a)– 6(c) in terms of height contours.

We also tested the PML method for a non-convective case where  $U_m = 0$ . Figure 7 represents the evolution of the  $L_2$  error. Again the error computed using only characteristic boundary conditions and second order Engquist boundary conditions is given for comparison. In this case the three stages come very early and by 2000 seconds the curves flatten out. As before, the PML performs better than the characteristic and Engquist boundary conditions. See Figures 8(a)–8(c) for the height contours of the Gaussian at different times. Note that since this is a non-convective case the center stays at the origin at all times.

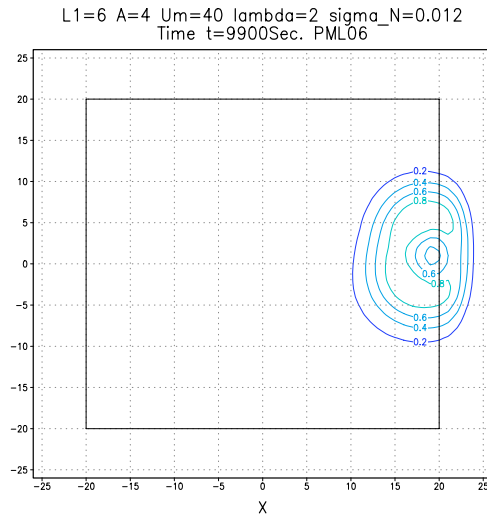
We carried out the same numerical experiments with another set of values of the absorption coefficients for the PML layer, i.e.  $\sigma_m$  and  $\beta$ . Figures 9–14(c) show the results of an experiment with  $\beta = 3$  and  $\sigma_m = 0.006$  and various values of mean flow speed. The results obtained for  $U_m = 30\text{m}/\text{sec}$  display a better separation between the different layer thicknesses of the PML domain. As in all previous cases the PML errors are smaller than those using the characteristic or Engquist boundary conditions. Figures 10(a)–10(c) show the height contours of the Gaussian at different times for a mean flow velocity of  $U_m = 30\text{m}/\text{sec}$ . There is no difference between the first two figures 10(a)–10(b) and the corresponding ones, figures 2(a)–2(b). The



(a) Same as Fig. 2(a) but for  $U_m = 40m/sec$ .



(b) Same as Fig. 4(a) but the computed result is given at  $t = 5400sec$ .



(c) Same as Fig. 4(a) but the computed result is given at  $t = 9900sec$ .

Figure 4:

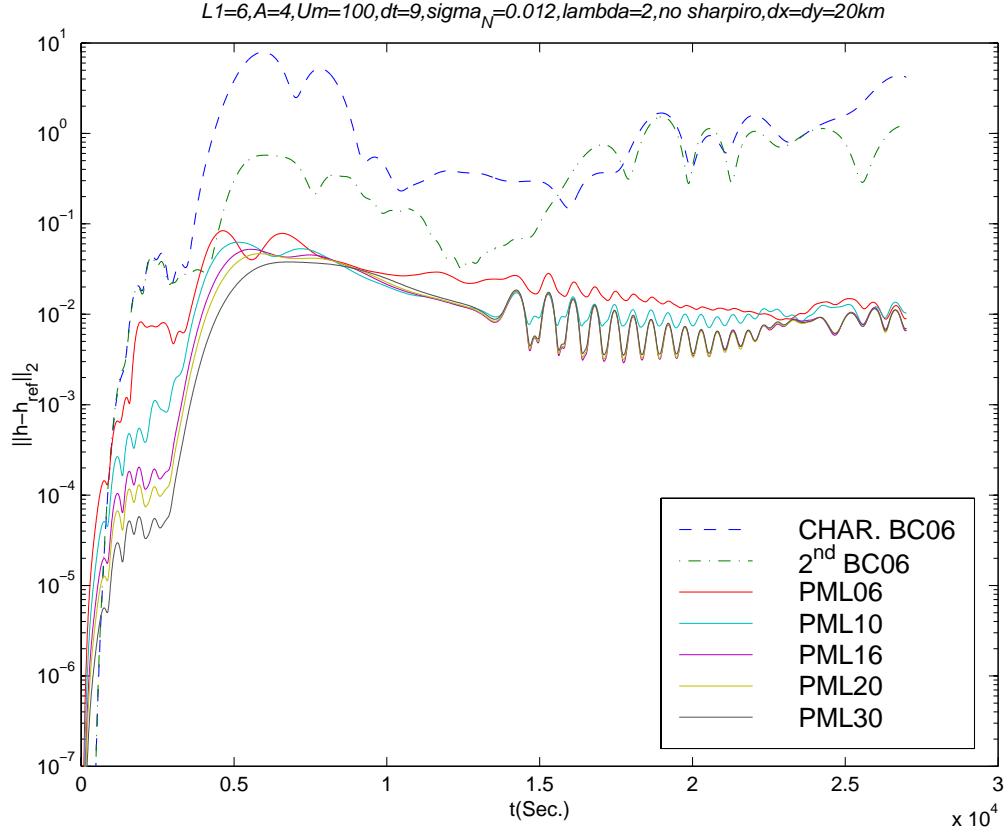


Figure 5: Same as Fig. 1 but for mean velocity  $U_m = 100m/sec$ .

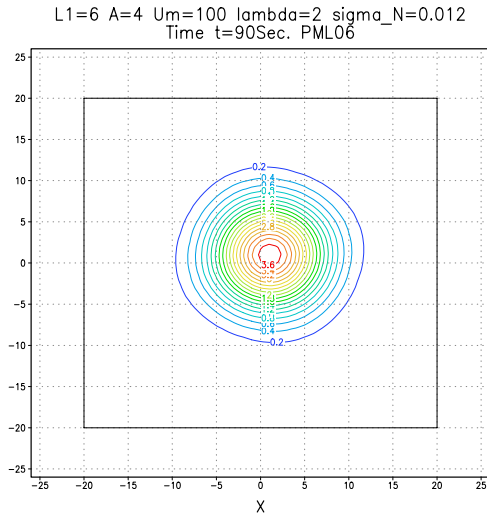
effect of the absorption coefficient manifest itself in Figure 10(c) as a wider vortex whose right boundary closer to the right boundary of the domain.

Figure 11 represents the evolution of the  $L_2$  error in the height field for  $U_m = 40m/sec$ . The error computed using only characteristic boundary conditions or second order Engquist boundary conditions is given for comparison. Again these two didn't perform as well as the PML schemes. Figures 12(a)–12(c) show the height contours of the Gaussian at different times. As in the previous experiment, we see the same effect of the absorption coefficients on the height contours at the three times, i.e. only at the last time plotted.

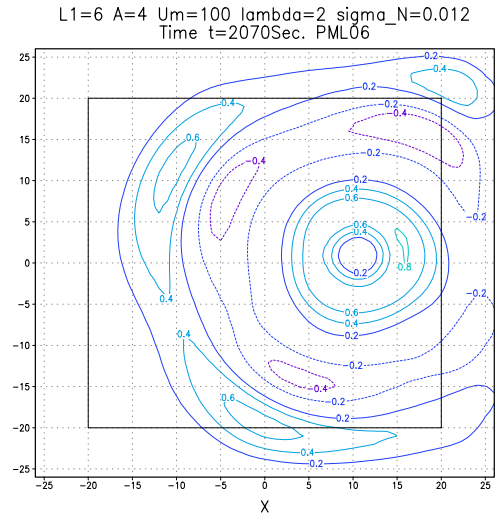
Figure 13 represents the evolution of the  $L_2$  error for  $U_m = 100m/sec$ . The error computed using only characteristic boundary conditions or second order Engquist boundary conditions are, as in other experiments, the largest. The case with the smallest ( $6\Delta x$ ) thickness of PML layer is giving as large errors as the second order Engquist boundary condition when the time is between 5000 to 10000 seconds. This is the only case where the PML layer has a difficulty due to the lower value of  $\sigma_m$  tested combined with the high value of the mean flow field. See Figures 14(a)–14(c) for the height contours of the Gaussian at different times. A numerical analysis of the propagation of fast gravity waves is given in Appendix A.

All the other results obtained show that the PML layer experiments are successful in terms of reduced reflectivity when compared to either characteristic well-posed boundary conditions or to the second order Engquist boundary conditions for the nonlinear shallow-water equations model.

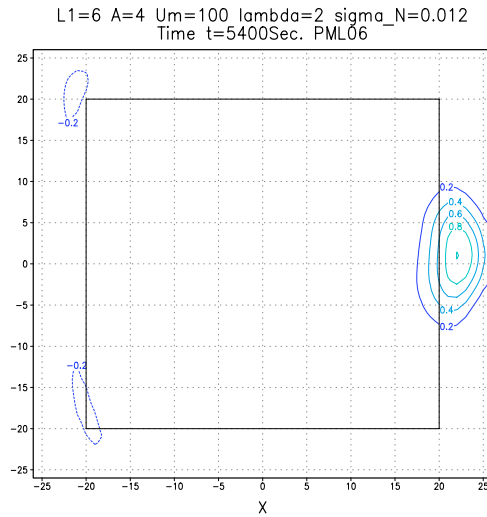
To measure the efficiency of the PML scheme in the inflow layer, we plotted (Figure 15) the  $L_2$  error in the height field along the line  $x = -18$  (in the left layer) for the same case described in Figure 1. The maximum error is smaller for the characteristic and Engquist second order boundary conditions. As for the PML, the only difference is at the onset of the third stage when curves flatten out.



(a) Same as Fig. 2(a) but for  $U_m = 100m/sec$ .



(b) Same as Fig. 6(a) but the computed result is given at  $t = 2070sec$ .



(c) Same as Fig. 6(a) but the computed result is given at  $t = 5400sec$ .

Figure 6:

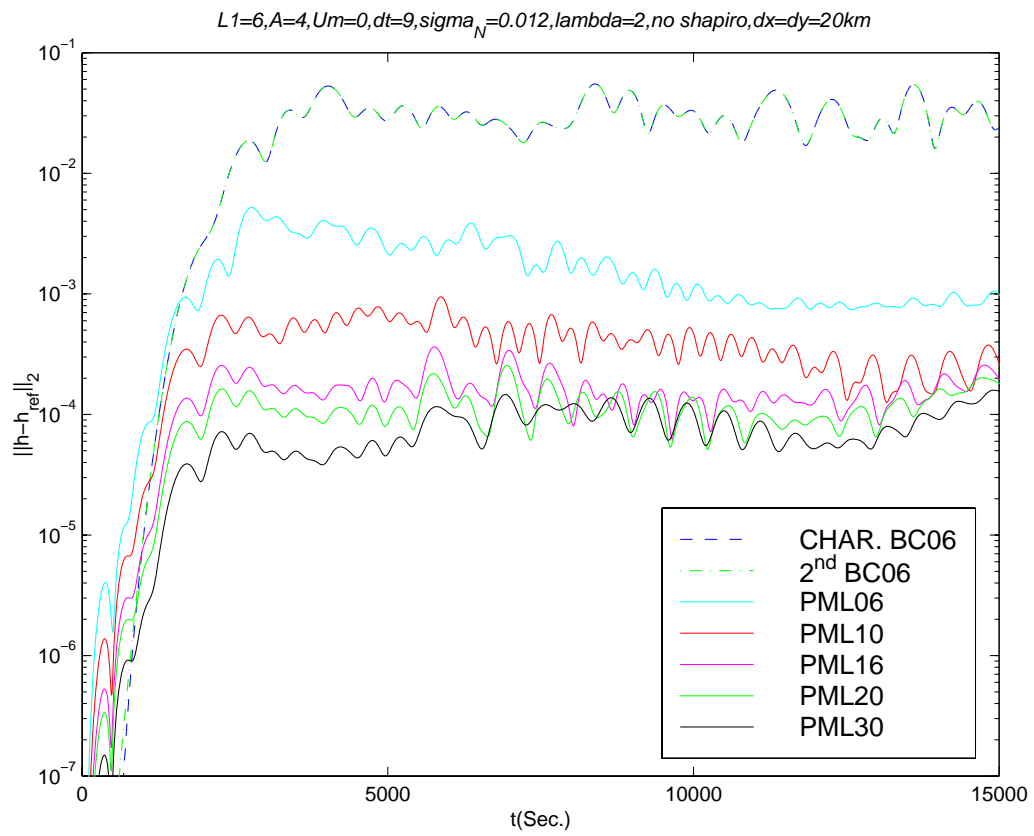
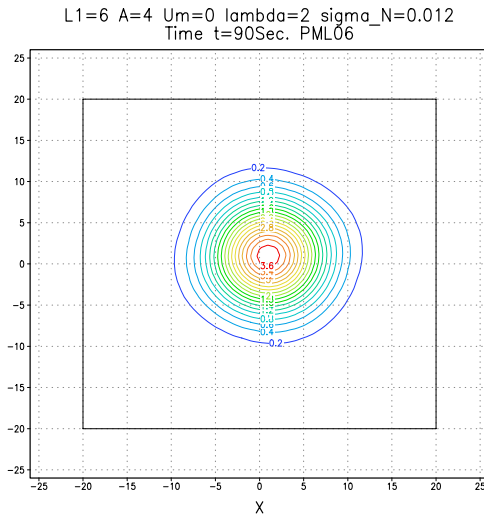
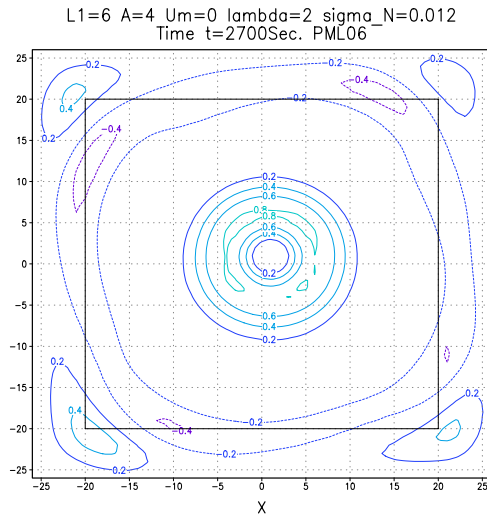


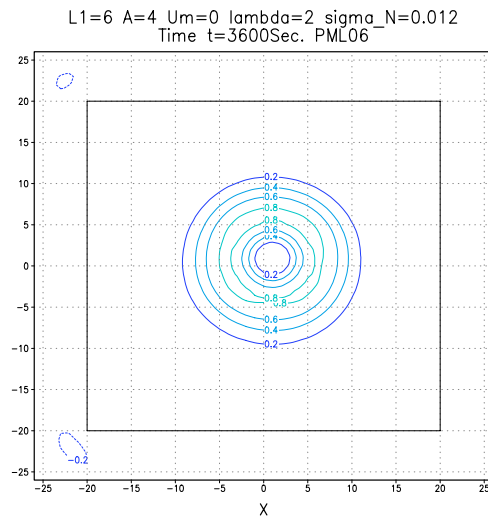
Figure 7: Same as Fig. 1 but for the non-convective case when  $U_m = 0\text{m/sec}$ .



(a) Same as Fig. 2(a) but for the non-convective case when  $U_m = 0m/sec.$  and result is given at  $t = 90sec.$



(b) Same as Fig. 8(a) but the computed result is given at time  $t = 2700sec.$



(c) Same as Fig. 8(a) but the computed result is given at  $t = 3600sec.$

Figure 8:

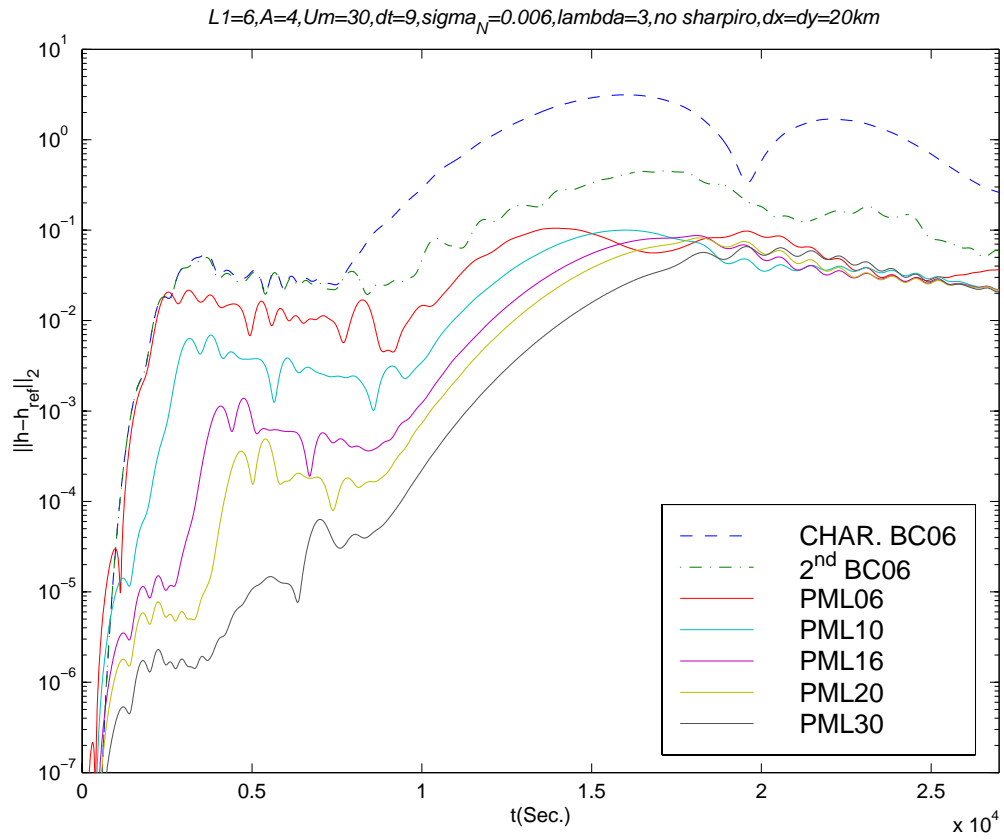
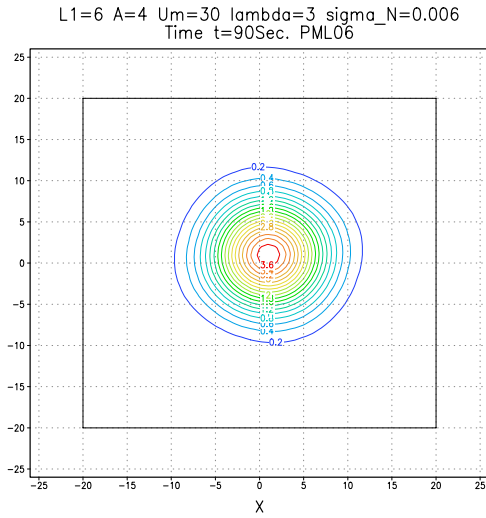
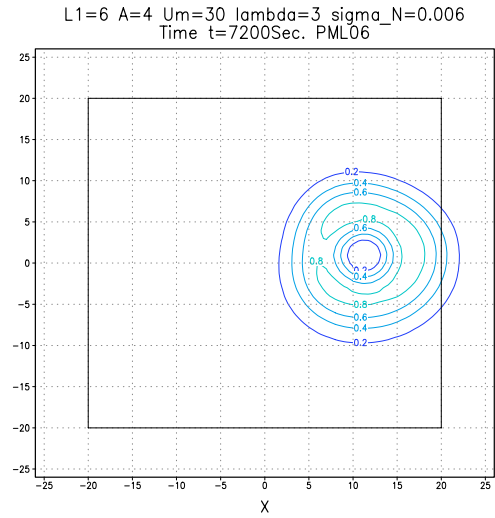


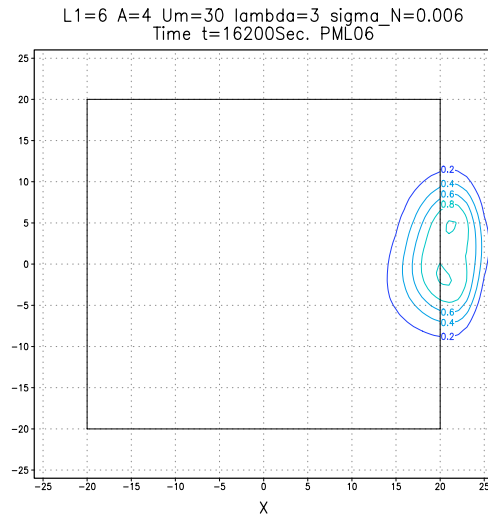
Figure 9: The evolution of the  $L_2$  height error along the line  $x = 18$  for various PML layer thicknesses for  $U_m = 30\text{m/sec}$  but for PML layer parameters  $\sigma_N = 0.006$  and  $\lambda = 3$ . The error computing only characteristic or second order Engquist-Majda boundary conditions is given for comparison.



(a) Same as Fig. 2(a) but for  $\sigma_N = 0.006$  and  $\lambda = 3$  and  $U_m = 30m/sec$ .



(b) Same as Fig. 10(a) but the computed result is given at time  $t = 7200sec$ .



(c) Same as Fig. 10(a) but the computed result is given at  $t = 16200sec$ .

Figure 10:

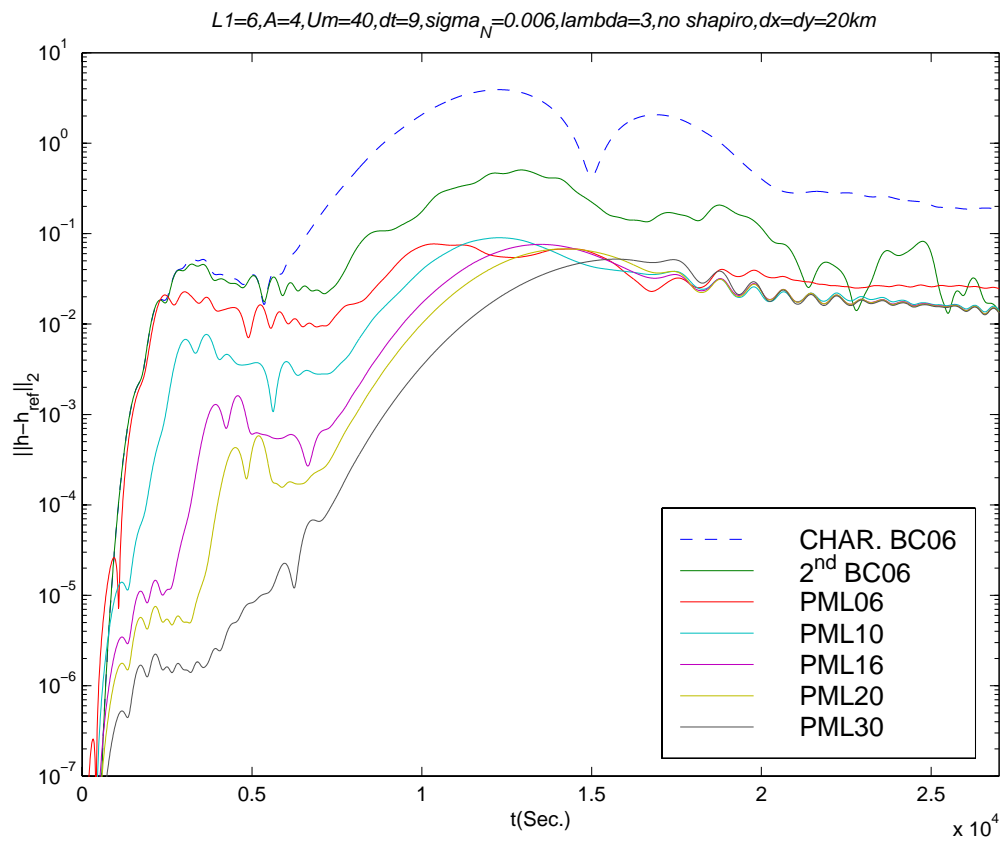
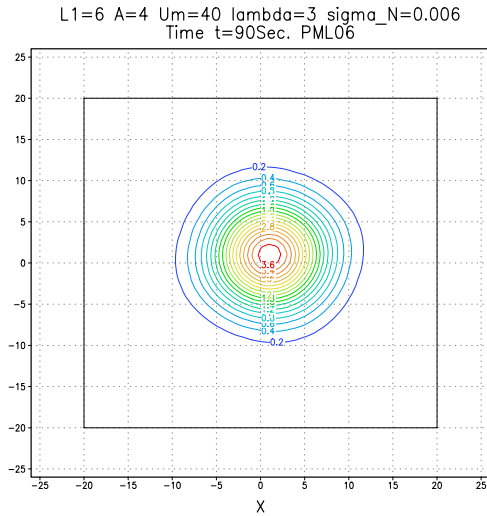
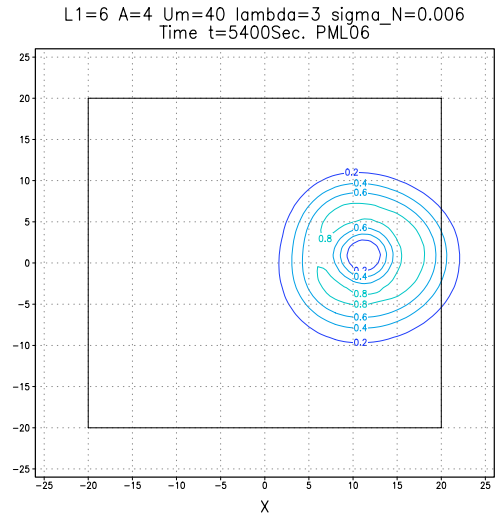


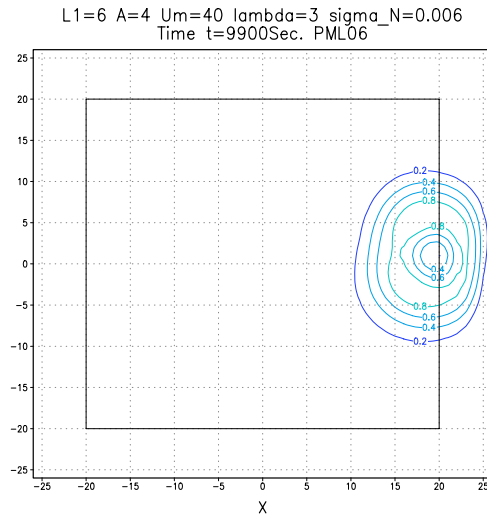
Figure 11: Same as Fig. 9 but for  $U_m = 40\text{m/sec}$ .



(a) Same as Fig. 10(a) but for  $U_m = 40m/sec.$  and result is given at  $t = 90sec.$



(b) Same as Fig. 12(a) but the computed result is given at time  $t = 5400sec.$



(c) Same as Fig. 12(a) but the computed result is given at  $t = 9900sec.$

Figure 12:

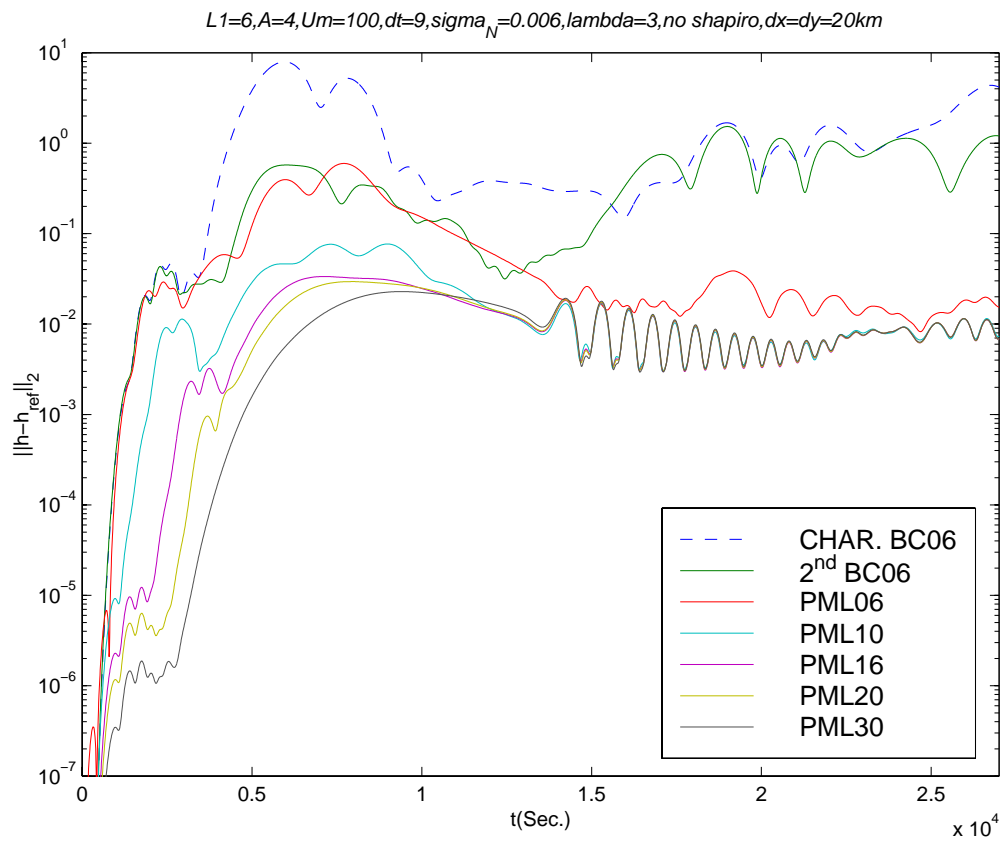
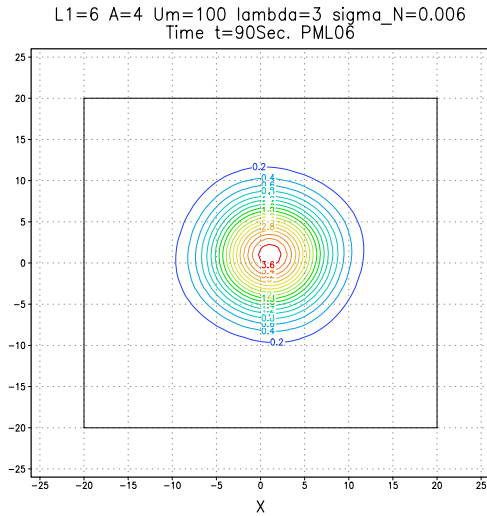
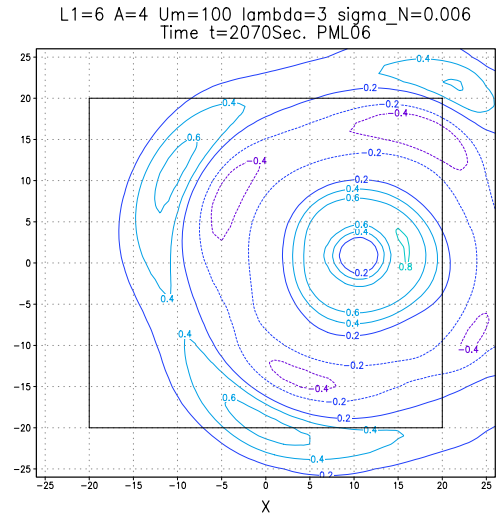


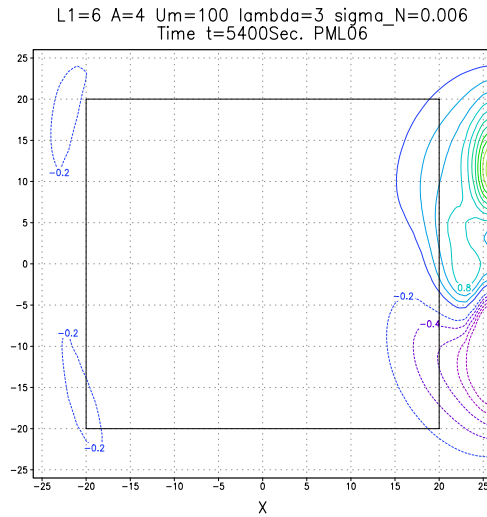
Figure 13: Same as Fig. 9 but for  $U_m = 100\text{m}/\text{sec}$ .



(a) Same as Fig. 12(a) but for  $U_m = 100m/sec.$  and result is given at  $t = 90sec.$



(b) Same as Fig. 14(a) but the computed result is given at time  $t = 2070sec.$



(c) Same as Fig. 14(a) but the computed result is given at  $t = 5400sec.$

Figure 14:

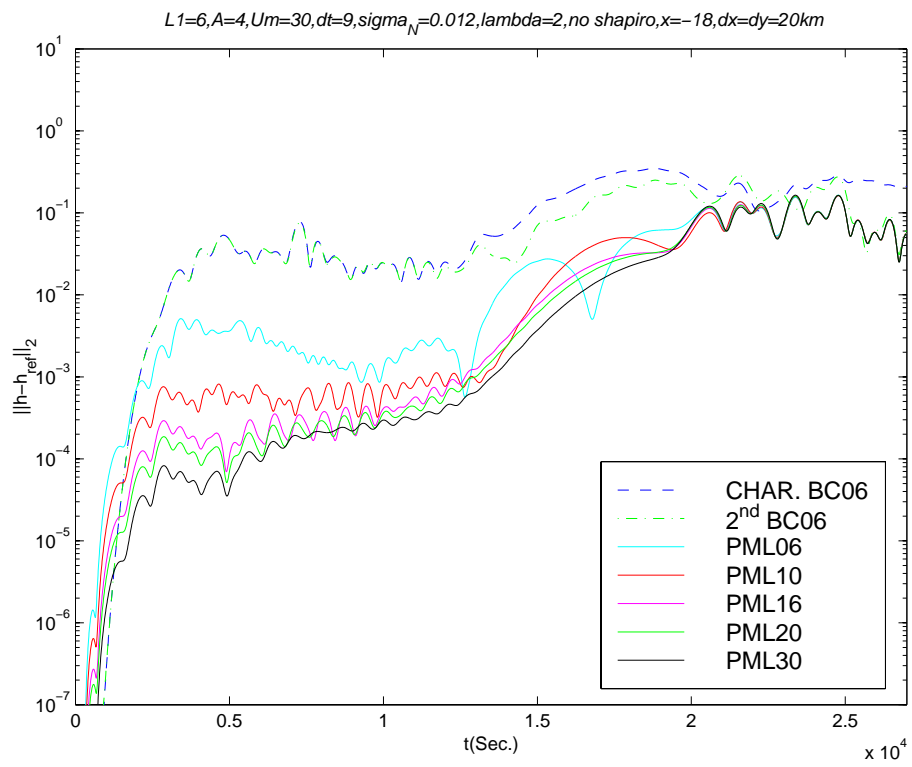


Figure 15: Same as Fig. 1, but for the inflow layer case  $x = -18$ .

### 3 Summary and conclusions

In this paper we have described and implemented the PML split equations approach for the nonlinear shallow water equations based on an explicit Miller-Pearce scheme finite difference discretization. We have derived the numerical method and developed the code for a rectangular grid domain. The results obtained without using any filters show the robustness of the method. Contrary to results obtained by Hu (1996), using a Shapiro 8-th order filter has negligible effects in our case.

Extensive numerical testing with an advected Gaussian pulse has shown that the PML boundary conditions radiates out the waves efficiently. Comparison with a set of characteristics well posed boundary conditions as well as the second order Engquist-Majda absorbing boundary conditions show that the PML scheme outperforms the characteristic boundary condition as well as the second order Engquist-Majda absorbing boundary conditions in terms of accuracy, while increasing the width of the PML layer leads to significant increase in accuracy.

The research carried out here has a natural extension to the formulation of boundary conditions for advanced mesoscale models, such as the MM5 and the new MRF models, and promises to improve upon the combination of nudging and sponge layer presently used in such models.

Issues of computational efficiency combined with numerical experience show that sizable benefits are already obtained with the present split-version of the nonlinear shallow water equations with a PML layer of a width not exceeding 16 cells, a fact which matches practical experience in mesoscale meteorology.

Work with PML in the framework of mesoscale models will mean that gravity waves can not only leave the domain but also enter it without hindrance. The fields imposed by the PML must be well balanced - since while the host fields are well-balanced on their own grid - subsequent interpolation to the guest model may upset the balance (McDonald 2001b).

Our results are encouraging and constitute a step towards using the PML transparent boundary conditions for full 3D atmospheric and ocean models. One avenue to achieve this goal is to implement the PML boundary conditions to a 3D multi-layer shallow water equations model as a way to proceed towards full 3D models. This can be done for the linearized hydrostatic equations by carrying out a normal mode decomposition yielding a shallow water equation for each vertical mode.

Development of a non-split version of both the linearized and the nonlinear version of the shallow water equations based on ideas put forward by Abarbanel and Gottlieb (1998), Abarbanel *et al.* (1999) and Hesthaven (1998) is presently also being investigated.

### Acknowledgements

The first author would like to express his gratitude for the support extended to him by the Center of Excellence (COE) at Florida State University during part of the write-up of this paper. This is a contribution from the climate institute, a center of excellence funded by the FSU research foundation. He also acknowledges support from NSF grant ATM-97B1472 managed by Dr. Pamela Stephens. He would also like to express his gratitude for the support and encouragement provided to him during his short stay at NCAR, fall 1999 made possible by DR Ying-Hwa Kuo, Head Mesoscale Prediction Group and by Dr Joseph Klemp, Head Mesoscale Dynamics Group both at NCAR/MMM. The expert programming help provided by Dr. Zhuo Liu during the implementation stages at CSIT is gratefully acknowledged. The useful discussion with Dr. Sajal K. Kar is acknowledged. The secretarial support and the expert librarian support at NCAR is also acknowledged.

## References

- [1] Abarbanel, S. and D. Gottlieb, 1997: A mathematical analysis of the PML method, *J. Comput. Phys.*, **134**, 357-363.
- [2] Abarbanel, S. and D. Gottlieb, 1998: On the construction and analysis of absorbing layers in CEM, *Appl. Numer. Math.*, **27**, 331-340.
- [3] Abarbanel, S., Gottlieb, D. and J. S. Hesthaven, 1999 : Well-posed perfectly matched layers for advective acoustics, *J. Comput. Phys.*, **154**, 266-283.
- [4] Berenger, J.-P., 1994: A perfectly matched layer for the absorption of electromagnetic waves, *J. Comput. Phys.*, **127**, 185-200.
- [5] Clement, A., 1996: Coupling of two absorbing boundary condition for 2D time-domain simulation of free surface gravity waves, *J. Comput. Phys.*, **126**, 139-159.
- [6] Collino, F., 1996: Perfectly matched absorbing layers for paraxial equations, *J. Comput. Phys.*, **131**, 164-180.
- [7] Darblade, G., Baraille, R., le Roux, A.-Y., Carton, X. and D. Pinchon, 1997: Conditions limites non réfléchissantes pour un modèle de Saint-Venant bidimensionnel barotrope linéarisé, *C. R. Acad. Sci. Paris*, **324**, 485-490.
- [8] Davies, H. C., 1976 : A lateral boundary formulation for multilevel prediction models, *Quart. J. Roy. Meteor. Soc.*, **102**, 405-418.
- [9] Davies, H. C., 1983 : Techniques for limited area modeling. *Seminar 1983: numerical methods for weather prediction. ECMWF, 5-9 September 1983*, 213-236.
- [10] Davies, H. C., 1985 : Limitations of some common lateral boundary schemes used in regional NWP models, *Mon. Wea. Rev.*, **111**, 1002-1012.
- [11] Durrant, D. R., Yang, M. J., Sinn, D. N. and R. G. Brown, 1993: Toward more accurate wave permeable boundary conditions, *Mon. Wea. Rev.*, **121**, 604-621.
- [12] Elvius, T., and A. Sundstrom, 1973: Computationally efficient schemes and boundary conditions for a fine mesh barotropic model based on the shallow-water equations, *Tellus*, **25**, 132-156.
- [13] Engquist, B. and A. Majda, 1977 : Absorbing boundary conditions for the numerical simulation of waves, *Math. Comp.*, **31**, no 139, 629-651.
- [14] Engquist, B. and A. Majda, 1979 : Radiation boundary conditions for acoustic and elastic wave calculations, *Comm. Pure. Appl. Math.*, **32**, 313-357.
- [15] Givoli, D., 1991: Nonreflecting boundary conditions, *J. Comput. Phys.*, **94**, 1-29.
- [16] D. Givoli and J. B. Keller, 1989: A Finite element method for large domains, *Comput. Meths. Appl. Mech. Eng.*, **76** , 41-66.
- [17] D. Givoli and I. Harari, guest editors, 1998: Exterior problems of wave propagation, Special issue of *Computer Methods in Applied Mechanics and Engineering*, **164(1-2)**, 272 p.
- [18] Goodrich, J.W. and T. Hagstrom, 1997 : A comparison of two accurate boundary treatments for computational aeroacoustics. AIAA paper 97-1585.11pp.
- [19] Gustafson, B., and A. Sundstrom, 1978: Incompletely parabolic problems in fluid dynamics, *SIAM J. Appl. Math.*, **35**, 343-357.

- [20] Haltiner, G. J. and R. T. Williams, 1980: Numerical Prediction and Dynamic Meteorology, John Wiley & Sons, New York.
- [21] Harari, I., Slavutin, M. and E. Turkel, 2000: Analytical and numerical studies of a finite element PML for the Helmholtz equation, *J. Comp. Acoustics*, **8**, 121-137.
- [22] Hayder, M. E. and H. L. Atkins, 1997: Experience with PML boundary conditions in fluid flow computation in T.L. Gears Ed.. Collection of Abstract of Symposium on computational methods for unbounded domains. Univ. of Colorado at Boulder, July 27-31 (Kluwer Academic Press) to appear.
- [23] Hayder, H. E., Hu, F. Q. and M. Y. Hussaini, 1999 : Towards perfectly absorbing boundary conditions for Euler equations, *AIAA Journal*, **37**, no 8 , 912-918.
- [24] Hesthaven, J. S., 1998 : On the analysis and construction of perfectly matched layers for the linearized Euler equations, *J. Comput. Phys.*, **142**, 129-147.
- [25] Higdon, R. L., 1986: Absorbing boundary conditions for difference approximations to the multi-dimensional wave equation. *Mathematics of Computation* ,**47**, No. **176**,437-459.
- [26] Holstad, A. and Lie, I., 2001: Transparent boundary conditions using a mixed finite element formulation of the shallow water equations, Norwegian Met. Inst. (DNMI), Research Report No. 120, 48 pp.
- [27] Hu, F. Q., 1996 : On absorbing boundary conditions for linearized Euler equations by a perfectly matched layer, *J. Comput. Phys.*, **129**, 201-216.
- [28] Israeli, H. and S. A. Orszag, 1981 : Approximation of radiation boundary conditions, *J. Comput. Phys.*, **41**, 115-135.
- [29] Jones, R.G., J.M. Murphy and M. Noguer, 1995: Simulation of a climate change over Europe using a nested regional climate model. I: Assessment of control climate including sensitivity to location of lateral boundary conditions, *Q. J. Roy. Met. Soc.*,**121**, 1413-1499
- [30] Kallberg, Per, 1977: Test of a boundary relaxation scheme in a barotropic model, ECMWF Res. Dept Internal Report No.3, 21pp.
- [31] Kalnay, E., 2001: Numerical Weather Forecasting and Predictability, Cambridge University Press, Cambridge, MA.
- [32] Kar, S. K. and R. P. Turco, 1995 : Formulation of a lateral sponge layer for limited-area shallow-water models and an extension for the vertically stratified case, *Mon. Wea. Rev.*, **123**, 1542-1559.
- [33] Karni, S., 1996: Far field filtering operators for suppression of reflections from artificial boundaries, *SIAM J. Numerical Anal.*, **33**, 1014-1047.
- [34] Kosloff, R. and D. Kosloff, 1986: Absorbing boundaries for wave propagation problems, *J. Comput. Phys.*, **63**, 363-376.
- [35] Lehmann, R., 1993: On the choice of relaxation coefficients for Davis lateral boundary scheme for regional weather prediction models, *Meteor. Atmos. Phys.*, **53**, 1-14.
- [36] Lie, I., 2001 : Well-posed transparent boundary conditions for the shallow water equations, *Appl. Numer. Math.*. To appear.
- [37] McDonald, A., 1997: Lateral boundary conditions for operational regional forecast models: A review HIRLAM Technical Report No 32, 31pp.
- [38] McDonald, A., 2001a: A step toward transparent boundary conditions for meteorological models, Irish Met. Service, Technical Note No. 57, 22 pp.

- [39] McDonald, A., 2001b: Well posed boundary conditions for semi-Lagrangian schemes: The two dimensional case, HIRLAM Technical Report No. 47, 38 pp.
- [40] McDonald, A. and J.E. Haugen, 1992: A two-time level three dimensional, semi-lagrangian and semi-implicit grid point model. *Mon. Wea. Review*, **120**, 2603-2621
- [41] Metral, J. and O. Vacus, 1999: Well-posedness of the Cauchy problem associated with Berenger's system, *Comp. Rendus de L'Acad. des Sci. Serie I-Math.*, **328**, 847-852.
- [42] Miller, M. J. and R. P. Pearce, 1974: A three dimensional primitive equation model of cumulonimbus convection, *Quart, J. Roy. Met. Soc.*, **100**, 133-154.
- [43] Miller, M. J. and A. J. Thorpe, 1981: Radiation conditions for the lateral boundaries of limited area models. *Quart, J. Roy. Met. Soc.*, **107**, 615-628.
- [44] Olinger, J. and Sundstrom A., 1978 : Theoretical and practical aspects of some initial boundary value problems in fluid dynamics, *SIAM J. Appl. Math.*, **35**, no 3 , 419-447.
- [45] Perkey, D. J. and C. W. Kreitzberg, 1976 : A time-dependent lateral boundary scheme for limited area primitive equations models, *Mon. Wea. Rev.*, **104**, 744-755.
- [46] Rahmouni, A., 2000: A well-posed unsplit PML model for linearized Euler equations, *Comp. Rendus de L'Acad. des Sci. Serie I-Math.*, **331**, 159-164.
- [47] Tam, C. K. W., Aurialt, L. and F. Cambuli, 1998 : Perfectly matched layer as an absorbing boundary condition for the linearized Euler equations in open and ducted domains, *J. Comput. Physics*, **144**, 213-244.
- [48] Taylor ,M., 1981: Pseudo-differential operators, Princeton University Press.
- [49] Tsynkov, V. S., 1998 : Numerical solution of problems on unbounded domains. A review, *Applied Num. Math.*, **27**, 465-532.
- [50] Turkel, E., 1983: Progress in Computational Physics, *Computers and Fluids*, **11**, 121-144.
- [51] Turkel, E. and A. Yefet, 1998: Absorbing PML boundary layers for wave-like equations, *Appl. Numer. Math.*, **27**, 533-557.

## A Propagation of fast moving gravity waves for the Gaussian advection equation.

For the sake of simplicity, let us consider the advection equation with  $c > 0$ :

$$u_t + cu_x = 0 \quad \text{for } t > 0 \quad (\text{A.1})$$

where

$$u = e^{-\ln 2 \left(\frac{x}{L\Delta x}\right)^2} \quad (\text{A.2})$$

We discretize the equation using a simple centered difference :

$$\frac{du_l}{dt} = \frac{c}{2\Delta x}(-u_{l+1} + u_{l-1}) \quad (\text{A.3})$$

where  $l$  stands for the grid number. Using

$$u_j = e^{i(\omega t - j\alpha\Delta x)}, \quad (\text{A.4})$$

where

$$\omega = \frac{c}{\Delta x} \sin \alpha\Delta x \quad (\text{A.5})$$

and where

$$\alpha\Delta x \in [-\pi, \pi] \quad (\text{A.6})$$

We find that the group velocity of the dispersion relation is given by:

$$\frac{\partial\omega}{\partial\alpha} = c \cos(\alpha\Delta x) \quad (\text{A.7})$$

Let us now consider the range

$$0 \leq \alpha\Delta x \leq \frac{\pi}{2} \quad (\text{A.8})$$

which implies  $\cos(\alpha\Delta x) > 0$ . This means that all wave number components of the initial Gaussian which satisfy  $0 < \alpha\Delta x \leq \frac{\pi}{2}$  travel to the right, *i.e.*, in the positive  $x$ -direction.

However for

$$\frac{\pi}{2} \leq \alpha\Delta x \leq \pi, \quad \cos(\alpha\Delta x) < 0 \quad (\text{A.9})$$

*i.e.*,  $\frac{\partial\omega}{\partial\alpha} < 0$ . These wave numbers of the initial Gaussian travel to the left, *i.e.* in the negative  $x$ -direction.

The fastest wave propagating to the right is given by

$$\frac{\partial\omega}{\partial\alpha} = c \cos(0) = c \quad (\text{A.10})$$

for  $\alpha\Delta x = 0$  which is the long-wave number limit, whereas the fastest wave propagation speed to the left is given by:

$$\frac{\partial\omega}{\partial\alpha} = -c \quad (\text{A.11})$$

for  $\alpha\Delta x = \pi$  that is all the grid to grid waves travel at speed of  $-c$ .

Use of either a finer mesh or a higher order differencing method will yield a more accurate solution, with less short-wave numbers travelling to the left.

## B Engquist-Majda boundary conditions

The approach of Engquist and Majda (1977,1979) is based on the theory of pseudodifferential operators (see Taylor 1981). A sequence of local approximate nonreflecting boundary conditions (NRBC) of increasing order is obtained.

Consider first the 2-D wave equation in Cartesian coordinates :

$$\frac{1}{c^2}u_{tt} = u_{xx} + u_{yy} \quad (\text{B.1})$$

Substitute the exponential solution  $u = De^{i(-\omega t + k_1 x + k_2 y)}$  in (B.1) to obtain the dispersion relation

$$k^2 = k_1^2 + k_2^2 = \frac{\omega^2}{c^2} \quad (\text{B.2})$$

Consider a straight segment of the artificial boundary B with outward normal in the positive  $x$  direction. Denoting  $s = \frac{k_2}{k}$  (with  $|s| \leq 1$ ) we have from (B.2)

$$k_1 = \pm k \sqrt{1 - s^2} \text{ on B} \quad (\text{B.3})$$

where  $\pm$  represent outgoing and incoming waves, respectively. If we wish to obtain an equation on  $B$  admitting only outgoing waves, the branch corresponding to  $+$  sign is chosen.

If we consider (B.3) as 1-D dispersion relation of an equation

$$Pu = 0 \text{ on B} \quad (\text{B.4})$$

obtained by applying an inverse Fourier transform to (B.3) which is an exact relation on  $B$ . Since  $k_1 = k_1(s)$  is an irrational function of  $s$ ,  $P$  in (B.4) is not a differential operator but rather a pseudodifferential operator, which is nonlocal in both time and space.

Engquist and Majda (1977) approximate the nonlocal operator  $P$  by a local differential operator  $E$ . This is done by approximating  $\sqrt{1 - s^2}$  by a rational function (such as Pade approximants). By using rational approximations of increasing accuracy they obtain local boundary conditions  $E_m u = 0$  on  $B$  of increasing order  $m$ .

For the case above:

$$E_1 u = \left( \frac{\partial}{\partial x} - \frac{1}{c} \frac{\partial}{\partial t} \right) u \Big|_{x=0} = 0 \quad (\text{B.5})$$

$$E_2 u = \left( \frac{1}{c} \frac{\partial^2}{\partial x \partial t} - \frac{1}{c^2} \frac{\partial^2}{\partial t^2} + \frac{1}{2} \frac{\partial^2}{\partial y^2} \right) u \Big|_{x=0} = 0 \quad (\text{B.6})$$

In terms of the modified expression (B.1)  $u = e^{i(\sqrt{\xi^2 - \omega^2}x + \xi t + \omega y)}$ , we obtain the symbol of the boundary condition (see Engquist and Majda) as:

$$\frac{d}{dx} - i\xi \sqrt{1 - \frac{\omega^2}{\xi^2}}$$

which can be approximated as  $\sqrt{1 - \frac{\omega^2}{\xi^2}} = 1 + O(\frac{\omega^2}{\xi^2})$  at normal incidence ( i.e.  $\omega = 0$ ) where  $i\xi$  corresponds to  $\frac{1}{c} \frac{\partial}{\partial t}$  gives (B.5) - (B.6) .

The next approximation (either Taylor or Pade) to the square root is :

$$\sqrt{1 - \frac{\omega^2}{\xi^2}} = 1 - \frac{1}{2} \left( \frac{\omega^2}{\xi^2} \right) + O\left( \frac{\omega^4}{\xi^4} \right)$$

and multiplying by  $i\xi$  yields the symbol

$$i\xi \frac{\partial}{\partial x} + \xi^2 - \frac{1}{2}\omega^2$$

or

$$\left( \frac{1}{c} \frac{\partial^2}{\partial x \partial t} - \frac{1}{c^2} \frac{\partial^2}{\partial t^2} + \frac{1}{2} \frac{\partial^2}{\partial y^2} \right) u \Big|_{x=0} = 0.$$

## B.1 Application to linear shallow-water equations

The linearized shallow water equations assume the form of a system given by:

$$\frac{\partial \hat{w}}{\partial t} = \begin{pmatrix} a & 0 & c \\ 0 & a & 0 \\ c & 0 & a \end{pmatrix} \frac{\partial \hat{w}}{\partial x} + \begin{pmatrix} b & 0 & 0 \\ 0 & b & c \\ 0 & c & b \end{pmatrix} \frac{\partial \hat{w}}{\partial y} + \begin{pmatrix} 0 & f & 0 \\ -f & 0 & 0 \\ 0 & 0 & 0 \end{pmatrix} \hat{w}$$

Physical restrictions on the constants are :  $c > 0$  and  $0 < a^2 + b^2 < c^2$ . We assume the matrices are constant.

We diagonalize the normal matrix (multiplying  $\frac{\partial \hat{w}}{\partial x}$ ) by multiplying by  $\mathbf{U}^{-1}$  where the unitary map  $\mathbf{U}$  is

$$\mathbf{U} = \begin{pmatrix} \frac{1}{\sqrt{2}} & 0 & \frac{1}{\sqrt{2}} \\ 0 & 1 & 0 \\ -\frac{1}{\sqrt{2}} & 0 & \frac{1}{\sqrt{2}} \end{pmatrix}$$

and let  $w = \mathbf{U}^{-1} \hat{w}$  to obtain

$$\frac{\partial w}{\partial t} = \begin{pmatrix} a-c & 0 & 0 \\ 0 & a & 0 \\ 0 & 0 & a+c \end{pmatrix} \frac{\partial w}{\partial x} + \begin{pmatrix} b & -\frac{c}{\sqrt{2}} & 0 \\ -\frac{c}{\sqrt{2}} & b & \frac{c}{\sqrt{2}} \\ 0 & \frac{c}{\sqrt{2}} & b \end{pmatrix} \frac{\partial w}{\partial y} + \begin{pmatrix} 0 & \frac{f}{\sqrt{2}} & 0 \\ -\frac{f}{\sqrt{2}} & 0 & -\frac{f}{\sqrt{2}} \\ 0 & \frac{f}{\sqrt{2}} & 0 \end{pmatrix} w$$

We want to write this equation in the form

$$\frac{\partial w}{\partial x} = A \frac{\partial w}{\partial t} + E \frac{\partial w}{\partial y} + Bw$$

We get:

$$\frac{\partial w}{\partial x} = \begin{pmatrix} \frac{1}{a-c} & 0 & 0 \\ 0 & \frac{1}{a} & 0 \\ 0 & 0 & \frac{1}{a+c} \end{pmatrix} \frac{\partial w}{\partial t} + \begin{pmatrix} -\frac{b}{a-c} & \frac{c}{(a-c)\sqrt{2}} & 0 \\ \frac{c}{a\sqrt{2}} & -\frac{b}{a} & -\frac{c}{a\sqrt{2}} \\ 0 & -\frac{c}{(a+c)\sqrt{2}} & -\frac{b}{(a+c)} \end{pmatrix} \frac{\partial w}{\partial y} + \begin{pmatrix} 0 & -\frac{f}{(a-c)\sqrt{2}} & 0 \\ \frac{f}{a\sqrt{2}} & 0 & \frac{f}{a\sqrt{2}} \\ 0 & -\frac{f}{(a+c)\sqrt{2}} & 0 \end{pmatrix} w$$

Boundary conditions will depend upon whether we have linearized about an inflowing state, i.e.  $a < 0$  or about an outflowing state (with  $a > 0$ ). For the inflow case Engquist and Majda (1977) obtained a sequence of increasing order local nonreflecting boundary conditions

$$0 > \Lambda_1 = \frac{1}{a-c}$$

$$0 < \Lambda_2 = \begin{pmatrix} \frac{1}{a} & 0 \\ 0 & \frac{1}{a+c} \end{pmatrix}$$

The first absorbing approximation yields

$$\begin{pmatrix} w_1 \\ w_2 \end{pmatrix} \Big|_{x=0} = 0$$

and the second approximation

$$\frac{\partial w_1}{\partial t} + \frac{a}{\sqrt{2}} \frac{\partial w_2}{\partial y} - \frac{a}{c\sqrt{2}} f w_2 \Big|_{x=0} = 0$$

## C Sponge-layer approach

Relatively few studies were carried out for lateral sponge layers (LSL). Davies (1976,1985) has formulated LSLs that relax interior flows to the external flow at the boundaries making use of spatially varying sponge coefficients. These coefficients can be either specified empirically or determined optimally in some sense (see Davies 1985, and Lehmann 1993) by trying to minimize reflections of outgoing gravity-inertia waves.

Following Kar and Turco (1995), one can write the one-dimensional shallow-water equations linearized around a basic state as

$$\frac{\partial u}{\partial t} + g \frac{\partial h}{\partial x} = -\alpha u + \beta \frac{c}{H} h \quad (\text{C.1})$$

$$\frac{\partial h}{\partial t} + H \frac{\partial u}{\partial x} = \beta \frac{H}{c} u - \alpha h \quad (\text{C.2})$$

where  $H$  is the height of free surface from basic state,  $h$  is a deviation of height from  $H$  for a perturbed state,  $u$  is velocity perturbation in  $x$ -direction,  $c$  is the phase speed of surface gravity waves, i.e.  $c = \sqrt{gH}$ , and  $\alpha \geq |\beta|$  either positive or negative are the sponge layer coefficients. Introducing characteristic variables  $C^+$  and  $C^-$  defined by

$$C^+ = u + \sqrt{\frac{g}{H}} h$$

$$C^- = u - \sqrt{\frac{g}{H}} h$$

yields characteristic equations

$$\frac{\partial C^+}{\partial t} + c \frac{\partial C^+}{\partial x} = -(\alpha - \beta) C^+$$

$$\frac{\partial C^-}{\partial t} - c \frac{\partial C^-}{\partial x} = -(\alpha + \beta) C^-$$

Using normal mode solution of the form

$$(u, h) = \text{Re} \left[ \left( \hat{u}(x), \hat{h}(x) \right) e^{-i\nu t} \right] \quad (\text{C.3})$$

$\nu$  being the angular frequency, and substituting (C.3) in (C.1) - (C.2) we obtain  $\hat{u}(x), \hat{h}(x)$  which implies that we get

$$\hat{u}(x) = D e^{ik_1 x} + E e^{ik_2 x}$$

$$\sqrt{\frac{g}{H}} \hat{h}(x) = D e^{ik_1 x} - E e^{ik_2 x}$$

To create a sponge layer (for the non-discretized case) one expands the domain  $0 \leq x \leq L$  by an extent  $d$ , i.e. for a right boundary  $L \leq x \leq L + d$  using equations (C.1) - (C.2) with  $|\beta| \leq \alpha$ .

We define wave reflectivity as the ratio of complex-valued amplitudes of incoming part of the wave to the outgoing part of wave solution. Using normal mode solutions one obtains at  $x = L$

$$R = e^{-2\alpha d/c}$$

In the discrete case we have

$$\begin{aligned} \frac{\partial u_i}{\partial t} + \frac{g}{\Delta}(h_{i+\frac{1}{2}} - h_{i-\frac{1}{2}}) &= -\alpha_i u_i + \beta_i \frac{c}{H} \frac{h_{i+\frac{1}{2}} + h_{i-\frac{1}{2}}}{2} \\ \frac{\partial h_{i+\frac{1}{2}}}{\partial t} + \frac{H}{\Delta}(u_{i+1} - u_i) &= \tilde{\beta}_{i+\frac{1}{2}} \frac{H}{c} \frac{u_i + u_{i+1}}{2} - \tilde{\alpha}_{i+\frac{1}{2}} h_{i+\frac{1}{2}} \end{aligned}$$

where  $\tilde{\alpha}, \tilde{\beta}$  are sponge-layer coefficients at  $n$  points. Using same techniques, where the width of the sponge layer region  $L \leq x \leq L + d$  has  $n$  grid intervals, one obtains the reflectivity  $R$  in functional form as

$$R = F(n, \tilde{\alpha}, \tilde{\beta}, \tilde{k})$$

with  $\tilde{\alpha} = \frac{\alpha \Delta}{c}$ , and  $\tilde{\beta} = \frac{\beta \Delta}{c}$ .

Here  $\Delta$  is the mesh interval in the x-direction. Numerically, Kar and Turco (1995) obtained a satisfactory LSL for  $n = 6$ ,  $\alpha \approx \frac{0.5c}{\Delta}$  and chose empirically a value  $\frac{\alpha \Delta}{c} \geq \frac{3}{n}$ .

The LSL with selective damping works for gravity waves with horizontal phase speed  $c$  greater than basic-state zonal velocity.

In atmospheric sciences the limited-area model, called also the guest model, uses values supplied to the lateral boundaries by the host model, which usually has a coarser mesh- while the guest is the finer mesh limited-area model.

As sharp differences may arise between imposed boundary fields and adjacent mesh points in the limited-area domain a relaxation towards the host model fields is imposed in a zone close to the boundary, i.e. the interior fields are relaxed towards host model fields, in a sponge-layer zone close to the boundary.

In the case of the 1-D advection equation the scheme assumes the form:

$$\frac{\partial u}{\partial t}(x, t) + U_0 \frac{\partial \phi u}{\partial t}(x, t) = -K(x)(u(x, t) - u^E(x, t)) \quad (\text{C.4})$$

where  $u^E(x, t)$  is the externally prescribed field by the host and  $K(x)$  is a coefficient which is nonzero only in the sponge-layer close to the boundary varying from a large number on the boundary to zero on the interior beyond the sponge layer.

For  $U_0 = 0$  and  $K, u^E$  being constants we obtain

$$u(0)e^{-Kt} + u^E[1 - e^{-Kt}] \quad (\text{C.5})$$

i.e. for large  $K$  the solution approaches the external field while for  $K = 0$ , at the start of the sponge layer, the solution is unchanged.

To minimize spurious reflections at the boundary judicious choices of  $K$  and the width of the sponge layer have to be made. As shown in McDonald (1997) time discretization of (C.4) leads to

$$u_i = (1 - \alpha_i)u_i^I + \alpha_i u_i^E$$

with  $0 \leq \alpha_i \leq 1$ ,  $\alpha_1 = 0$  and  $\alpha_i = 0$  for lines beyond the relaxation width or sponge layer zone of  $n$  lines in width. Kallberg (1977) arrived at a value of  $\alpha_i = 1 - \tanh(\frac{i-1}{2})$  for a sponge layer with  $n = 8$  lines.

Other profiles for  $\alpha$  were put forward by Jones et al. (1995) using a linear profile of  $\alpha_i = 1 - \frac{i-1}{n}$ , with a value of  $n = 4$ . McDonald and Haugen (1992) proposed a cosine profile of the form

$$\alpha_i = \frac{1 + \cos \frac{(i-1)\pi}{n}}{2} \quad (\text{C.6})$$